*Geological Magazine*

**www.cambridge.org/geo**

# Geochemical characteristic of the Lutetian black shale (Bayburt, NE-Turkey): amount, nature, origin of organic matter and palaeo-environment conditions

Çiğdem Saydam Eker

Department of Geological Engineering, Faculty of Natural Sciences and Engineering, Gümüşhane University, Gümüşhane, Turkey

**Original Article**

**Cite this article:** Saydam Eker Ç. Geochemical characteristic of the Lutetian black shale (Bayburt, NE-Turkey): amount, nature, origin of organic matter and palaeo-environment conditions. *Geological Magazine* **161**(e11): 1–23. https://doi.org/10.1017/S0016756824000281

Received: 19 February 2024
Revised: 31 July 2024
Accepted: 9 September 2024

**Keywords:**
Lutetian shale; organic matter; saturated and aromatic biomarker; $^{13}C_{org}$ isotope; palaeoenvironmental conditions

**Corresponding author:**
Ç. Saydam Eker;
Email: csaydam@gumushane.edu.tr

**Abstract**

To define the amount, thermal maturity and type of organic matter (OM), a comprehensive analysis of major and trace elements, organic carbon isotope and organic geochemistry was conducted on Lutetian black shales found in the Everek (Bayburt) region of northeastern Turkey. Total organic carbon (TOC) levels in the shale samples range from 0.62% to 6.75%, and type II–III to type III kerogen is generated, displaying a combination of high terrigenous and low marine OM. The $\delta^{13}C$ values (ranging from –28.22‰ to –28.23‰), aromatic hydrocarbon compounds (methyl phenanthrene, dibenzothiophene, tri-aromatic and monoaromatic steroids), saturated hydrocarbon compounds (sterane and terpane), acyclic isoprenoids, n-alkane distribution (n-$C_{13}$–n-$C_{36}$) and inorganic geochemical characterization support that the black shales were deposited in a terrestrial-marine transition environment and had a high proportion of terrestrial OM with small amounts of marine OM preserved in relatively arid to hot climate and oxic to suboxic conditions. The analysis of biomarker thermal maturity markers, $T_{max}$ (ranging from 449–458 °C) and estimated vitrinite reflectance (varying from 0.92 to 1.08%) values suggest that the black shales have reached the oil window. As a result, black shales are thought to contain low to high amounts of TOC, have a mixed kerogen type, reach a high thermal maturity level and produce little hydrocarbons.

## 1. Introduction

Black shales are typically thin laminated dark-coloured sedimentary rocks with fine-grained particles (Wignall, 1994; Eric *et al.* 2023). The origin, palaeo-climatic conditions, palaeo-depositional environment, palaeo-salinity and palaeo-redox conditions may all be inferred from the geochemical composition of shales (McLennan *et al.* 1993, Tanaka *et al.* 2007; Liang *et al.* 2018; Li *et al.* 2020; Wu *et al.* 2021)

Everyone agrees that the world's petroleum supply will ultimately run out of resources. It makes sense for the government and energy sectors to rekindle their interest in oil shale as a viable alternative supply of oil or a complement to fuel (Cirilli *et al.* 2018; Spina *et al.* 2018 Ilevbare & Adeleye, 2023). Because they have the potential to be sources and reservoirs of hydrocarbon accumulation, black shale sedimentary rocks – also known as organic-rich mudstone and shale – are of enormous interest to people all over the world (Jarvie *et al.* 2007; Spina *et al.* 2021). Nonetheless, because of rising energy demands, both marine and continental black shales have drawn more interest from conventional and unconventional petroleum resource developers. It is well known that most black shale deposits were primarily deposited in anoxic bottom-water environments in marine and continental sedimentary basins and that they contain significant levels of organic matter (OM) – more than 1 weight per cent (Hakimi *et al.* 2011; Makeen *et al.* 2015; Hatem *et al.* 2016; Ahmed *et al.* 2022).

However, many variables, including continental weathering, biological productivity, clay mineralogy, sedimentation rates, sea level change, water column oxygen levels and depositional environment, severely restrict the accumulating of OM in shale (e.g. Li *et al.* 2008; Zonneveld *et al.* 2010; Bechtel *et al.* 2012; Shu *et al.* 2013; He *et al.* 2017; Zhang *et al.* 2019). Prior studies have exhibited that the primary causes of OM enrichment are the productivity of organisms as well as the preservation and resolution of OM (Calvert & Pedersen, 1993; Bordenave *et al.* 1993; Carroll & Bohacs, 1999). OM preservation is significantly influenced by redox conditions. Furthermore, there might be fluctuating restrictions on OM enrichments due to the terrigenous input and sedimentation rate. Some of the sources of Al and Ti are heavy minerals and aluminosilicate minerals. It is proposed that both components serve as reliable stand-ins for detrital inflow (Murphy *et al.* 2000). In addition, primary productivity is increased in warm,

humid climates that support biological growth (Meng *et al.* 2012; He *et al.* 2017; Li *et al.* 2019). This means that there is a definite relationship between climate and productivity.

Sediments provide good information on the palaeo-climate and palaeo-environment after several representatives, including elemental, isotopic and molecular organic geochemical ones, are investigated. These biomarkers are frequently employed in the reconstruction of palaeo-environmental conditions (Meyers & Ishiwatari, 1993; Meyers, 2003; Xie *et al.* 2004; Zhou *et al.* 2005; Ortiz *et al.* 2010 & 2021; Koralay 2021). N-alkanes are widely used for this purpose because the origin of n-alkanes in the lithological record can be inferred from their distribution, e.g. primary sources of short-chain n-alkanes ($C_{17}$ and $C_{19}$) are cyanobacteria and algae (Cranwell *et al.* 1987). Terrestrial plants have n-alkanes in their leaf wax that are richer in $C_{27}$ to $C_{31}$, while aquatic macrophytes have homologues of $C_{23}$ and $C_{25}$ predominating (Eglinton & Hamilton 1967; Ortiz *et al.* 2021). The $\delta^{13}C$ composition of certain chemicals has been utilized for palaeo-environmental interpretations. The $\delta^{13}C$ composition of individual n-alkanes provides more specific information on past variations in C3 and C4 plant abundance than the $\delta^{13}C$ of bulk OM. It has been utilized to deduce source inputs and biochemical pathways (Street-Perrot *et al.* 1997; Ficken *et al.* 1998; Huang *et al.* 2000; Sinninghe Damste *et al.* 2011; Sun *et al.* 2013).

The Lutetian sedimentary sequence outcropping in the Everek area (Bayburt) contains black shale layers in places. Since it is thought that these black shale levels may be rich in OM, it was found worth investigating. Eocene aged marl/shale outcropping around Çalıdere, approximately 20 km away from the Everek region, was previously examined to feature the OM and sedimentation environment and to evaluate its hydrocarbon production potential (Saydam Eker, 2022). With the previous study, approximate information was obtained about the type, amount and degree of maturation of OM in marl/shale. However, questions about productivity, the relationship between productivity and OM, the relationship between the palaeo-environment and its conditions and OM, the factors causing high $T_{max}$ and the basin model have not been answered due to the lack of aromatic biomarkers and major and trace element analyses.

The main purpose of this study is to define the amount of OM contained in black shales, kerogen type, maturation level of OM, source of OM and affecting factors based on organic geochemical analysis (Rock-Eval/TOC, stable carbon isotope, gas chromatography (GC), GC-mass spectrometry (GC-MS)). In addition, palaeo-climate, palaeo-productivity, palaeo-redox and palaeo-salinity conditions and therefore palaeo-depositional environment and conditions were interpreted based on inorganic (whole-rock trace and major elements analysis) and organic geochemical data of the black shales.

## 2. Geological setting

The Bayburt area is in the Eastern Pontides orogenic band of the Alpine–Himalaya fold system in northeastern Anatolia. The Carboniferous aged Pulur Metamorphic Massif, which comprises migmatite, amphibolite, gneiss, phyllite, marble, meta-chert and metavolcanic, is the oldest geological block in the Bayburt region. Upper Carboniferous–Permian rocks consist of the Carboniferous Cebre Rhyolite including high K calc-alkaline rhyolites and detrital rocks containing conglomerate, mature sandstone, limestone and shale (Topuz *et al.* 2004; Eyüboğlu *et al.* 2017; Dokuz *et al.* 2017). The Early Jurassic unit thickness varies between 1500 and 1800 m and consists of an alternation of conglomerate, sandstone, siltstone, marl, shale and tuffite. This alternation is accompanied by bands and lenses of red-coloured fossiliferous limestone, coal and acidic-basic rocks, dykes and sills. This sequence is unconformably layered above these basement rocks (Saydam Eker *et al.* 2015; Saydam Eker *et al.* 2016a). The Late Jurassic to Early Cretaceous aged limestone, which is separated into three units in the research region, is unconformably layered above these strata. Unit I is primarily made up of thick to medium-bedded grey and beige-coloured sandstone, gravel stone and sandy limestone; Unit II is made up of thick-bedded grey and beige-coloured oolitic, wackestone, packstone and grainstone and Unit III is mostly made up of thin-bedded yellow-coloured dolomite. Reefal limestones conformably overlie earlier limestone units, whereas the Upper Cretaceous series conformably overlies the carbonate rocks. Late Cretaceous rocks show great diversity lithological and have been examined under four different units. Unit I consists of an alternation of brown, yellowish sandstone, red pelagic limestone, mudstone and claystone. Unit II consists of andesite, basalt, andesitic-basaltic, tuff and tuffite. Unit III is a mélange and contains sandstone, marl, radiolarite, chert, serpentinite, gabbro, basalt and limestone blocks. Unit IV is a white, grey-coloured reef limestone and contains abundant coral (Keskin *et al.* 1990). Unit IV is overlain unconformably by the Pleistocene sedimentary rock, which is made up of marl, sandstone, sandy limestone and grey-coloured, thin, medium-layer pelagic limestone. Keskin *et al.* (1990) divided Eocene rocks into four formations named Sığırcı Formation (thickness varies between 275 and 470), Sırataşlar Formation (thickness about 750 m), Yazyurdu Formation (thickness varies between 250 and 300) and Rize Pluton (thickness varies between 800 and 1000). Sığırcı Formasyonu (the subject of this study) begins with basement conglomerate. Lutetian sedimentary rocks are classified as turbidite units, consisting of grey, brown and greyish-green thin- to thick-layered, fine- to medium-grained sandstones intercalated with marls and shales that are grey and dark grey in hue (Saydam Eker, 2012). There is also an upper interval of coal-containing claystone in some places (Saydam Eker *et al.* 2016b). Sırataşlar Formasyonu consists of grey, beige, yellow, dirty yellow, light green, coloured, medium-thick layered, limestone, sandstone, occasionally marl and sandy limestone levels. Yazyurdu Formasyonu is characteristic of volcano-clastic rocks composed of andesitic-basaltic rock, marl, sandstone and tuff. Rize Pluton generally consists of volcanic and plutonic rocks. The basaltic to andesitic rocks have an affinity for calc-alkaline to tholeiitic rocks, whilst the intrusive rocks are composed of granodiorite, tonalite and diorite. (Kaygusuz & Öztürk, 2015; Eyuboğlu *et al.* 2017; Gücer, 2021; Kaygusuz *et al.* 2022). Eocene rocks unconformably overlie Miocene rocks, which include limestone, marl, conglomerate, siltstone, sandstone and gypsum. Travertine is formed when carbonic acid-rich water percolates from rocks in limestone. The alluvium is from rounded and subrounded gravel, clay, silt and sand, mainly derived from non-altered sources and not chemically mature (Saydam Eker & Demirkol Kiliç, 2018; 2024), the older rocks are covered unconformably by Quaternary units (Figs. 1a, b, 2a).

## 3. Samples and methods

During the field study, a stratigraphic section was measured (Measured stratigraphic section= MSS) from Everek (about 40°7′59″ north and 40°22′59″east), where the Lutetian black shales are best exposed. The Everek measured stratigraphic section

https://doi.org/10.1017/S0016756824000281 Published online by Cambridge University Press

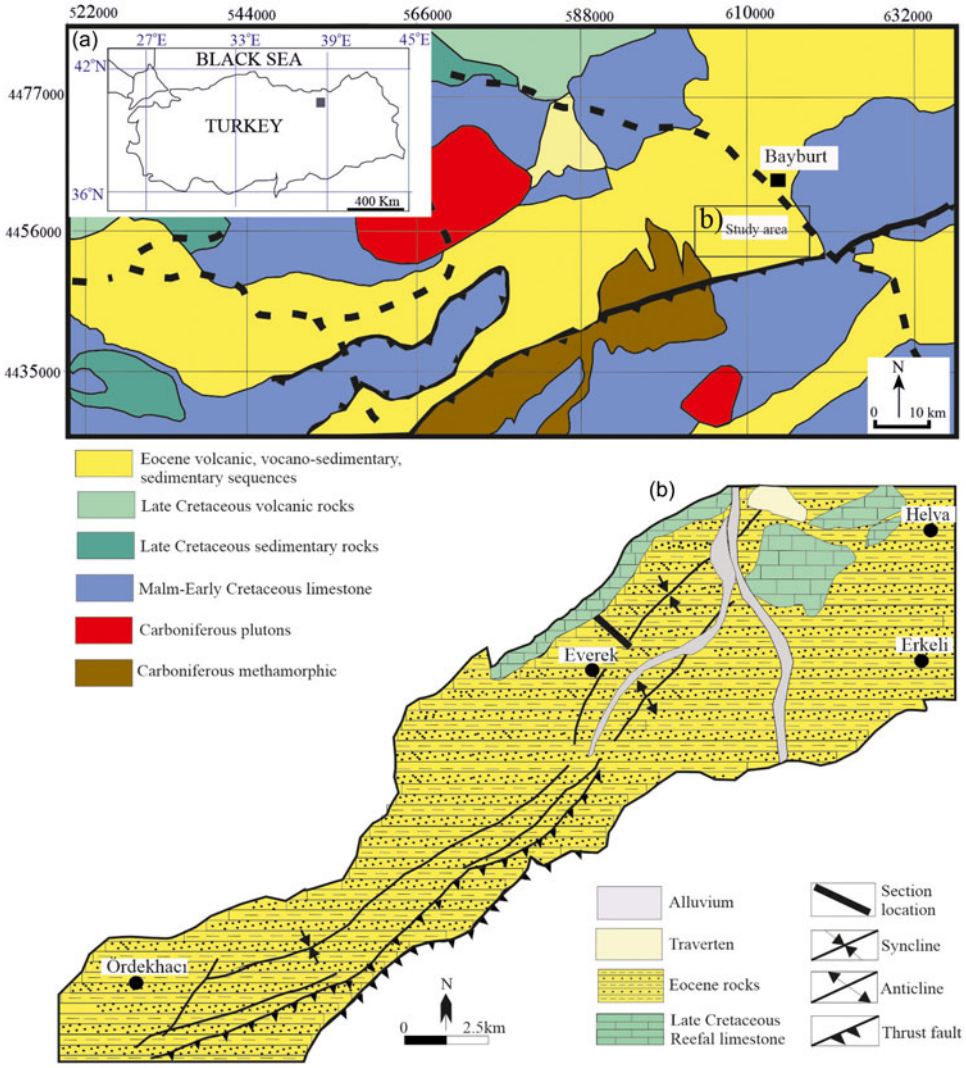


**Figure 1.** (Colour online) (a) Simplified geological map of the eastern Pontides (after Güven, 1993) and location map of the study area. (b) Geological map of the study area (after Musaoğlu, 1987).

starts with sandstones at the base and contains alternations of sandstone, marl and shale upwards (Fig. 2a). For geochemical analysis, 10 samples were collected from black shales (Fig. 2b). Whole-rock trace, major elements and Rock-Eval/TOC analyses were applied to 10 shale samples. Based on the results of the Rock-Eval/TOC analyses, stable carbon isotope ($\delta^{13}C$), GC–MS of aromatic and saturated biomarkers and GC analyses were also applied to two shale samples (E-15 and E-16, Fig. 2c, b).

### 3.a. Inorganic geochemistry analysis

At Vancouver, Canada's commercial Acme Analytical Laboratories Ltd. (now Bureau Veritas Minerals), major and trace elements were identified on ten shale samples. 0.2 g of sediment fused with 1.5 g of LiBO2 and dissolved in 100 ml of 5% HNO3 were used to evaluate the major and trace element compositions using inductively coupled plasma mass spectrometry (ICP-MS) and ICP optical emission spectrometry. Dried samples were heated to 1,000 °C for 15 minutes to calculate loss on ignition. For trace elements, the detection limits ranged from 0.1 ppm to 10 ppm. Calibration and verification standards together with reagent blanks was added to the sample sequences. In-house certification of STD SO-18 was performed against 38 certified reference materials, which included CANMET SY-4 as well as established external standards USGS AGV-1, G-2, GSP-2 and W-2. The analytical precision exceeds 4%.

Since chemical weathering is closely related to palaeo-climate, chemical index alteration (CIA) was used. Nesbitt & Young (1982) first proposed CIA, which is widely used to investigate the palaeo-climate (Feng *et al.* 2003; Yadav & Rajamani, 2004; Goldberg & Humayun, 2010; Wang *et al.* 2017; Xu & Shao, 2018; Liang *et al.* 2020; Saydam Eker & Arı, 2020). The CIA is calculated using the following formula:

$$\mathrm{CIA} = \mathrm{mole}[\mathrm{Al_2O_3}/(\mathrm{Al_2O_3} + \mathrm{CaO} + \mathrm{Na_2O} + \mathrm{K_2O})] \times 100 \quad (1)$$

$$\mathrm{CaO}* = \mathrm{mole\ CaO\ mole\ P_2O_5} \times 10/5 \quad (2)$$

Where CaO* indicates the sum of CaO in silicates.

Furthermore, the distribution and content of a few main and trace elements in sedimentary strata may reveal palaeo-climatic changes (Hu *et al.* 2017). Some research effectively used the C-value as a proxy for climate change (e.g. Zhao *et al.* 2007; Fu *et al.* 2016; Wang *et al.* 2017)

https://doi.org/10.1017/S0016756824000281 Published online by Cambridge University Press

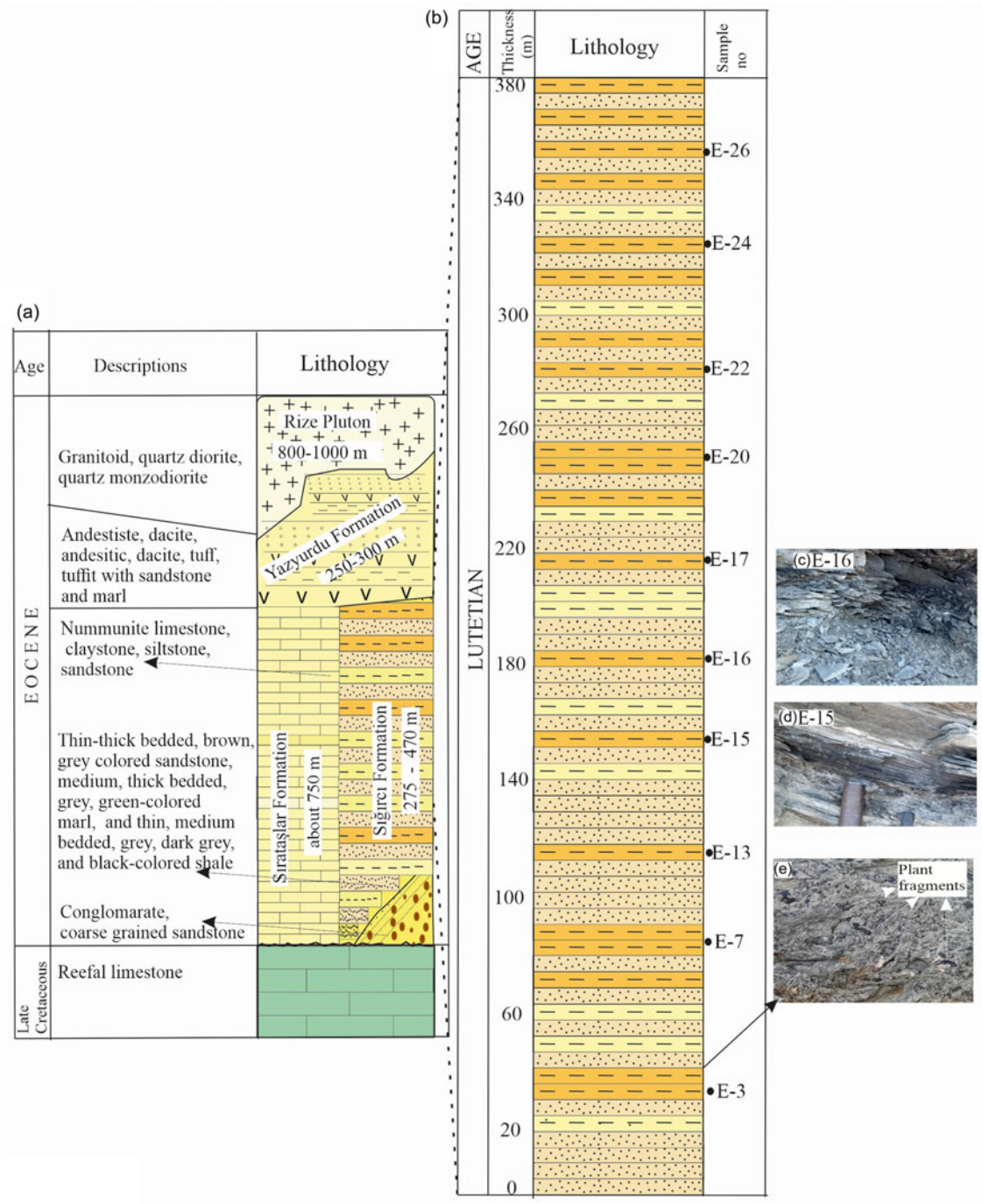


**Figure 2.** (Colour online) (a) Stratigraphic section of Eocene rocks, (b) measured stratigraphic sections of Lütetian detrital rocks, (c) and (d) photographs of black shale and (e) photograph of plant fragments.

The C-value is calculated by the following formula:

$$C - \text{value} = \Sigma(Fe + Mn + Cr + Ni + V + Co)/\Sigma(Ca + Mg + Na + K + Sr + Ba) \quad (3)$$

### 3.b. Stable carbon isotope analysis

Two samples of black shale (E-15 and E-16 samples containing the highest TOC) underwent stable carbon isotope analysis ($\delta^{13}C$). A system called Elementary Vario Pyro Cube Isoprime Vision Elemental Analyzer– Isotope Ratio Mass Spectrometry (EA-IRMS) was used to perform this analytical technique. Calibration was performed using Sorghum Flour, EMA-PI and NB-22-approved reference materials. The isotope data for nitrogen, carbon and sulphur are provided by Vienna Canyon Diablo Troilite VCDT, Vienna Pee Dee Belemnite (VPDB) and AIR. Every sample undergoes at least two analyses. The Turkish Petroleum Corporation's Oil and Organic Geochemistry Laboratory (TPAO, Ankara) performed the analyses.

https://doi.org/10.1017/S0016756824000281 Published online by Cambridge University Press

### 3.c. Organic geochemistry analysis

Rock-Eval 6 equipment fitted with a TOC module has been used for Rock-Eval pyrolysis/TOC analysis of shale materials. The samples were heated at a rate of 25 °C per minute from 300 °C (hold time: 3 min) to 650 °C. For oxidation, the crushed sediment was heated at a rate of 25 °C per minute from 400 °C (hold time 3 min) to 850 °C (hold time 5 min). Two samples (E-15 and E-16) were subjected to a 40-hour Soxhlet extraction process using dichloromethane ($CH_2C_{l2}$) to yield extracts. An Agilent 6850 gas chromatograph fitted with a flame photometric detector and flame ionization detector was used to examine the entire extract. Helium was used as the carrier gas for a fused capillary column (100m, 0.25 mm i.d.) coated with cross-linked dimethylpolysiloxane (JandW, 0.50 $^0$m film thickness) used for separation. The oven's temperature was set to rise at a rate of 4 °C per minute from 40 °C (hold time: 8 min) to 270 °C (hold time: 60 min). Using liquid chromatography, the extract samples were divided into fractions containing Nitrogen, Sulfur, Oxygen (NSO) compounds, aromatic hydrocarbons and saturated hydrocarbons. To elute the fractions, N-hexane, toluene and methanol were utilized, in that order. The two samples (E-15 and E-16) with the highest extract were subjected to GC-MS studies. Shale extracts' saturated fractions were used for the GC-MS analyses. An Agilent 5975C quadrupole mass spectrometer was connected to an automated liquid sampler (7683 B) and a gas chromatograph (7890 A). An HP-1MS fused silica capillary column measuring 60 m in length, 0.25 mm in diameter and 0.25 µm in film thickness was fitted with the gas chromatograph. The carrier gas in this case was helium. Programming for the oven temperature included a range of 50 °C (hold time 10 min), 200 °C (hold time 15 min), 250 °C (hold time 24 min) and 280 °C (hold time 24 min) at 2 °C/min. At last, the oven was raised to 290 °C (hold time: 40 min) at a rate of 1 °C per minute. At a source temperature of 300 °C and an ionization energy of 70 eV, the mass spectrometer was run in the EI mode. Biomarker contents are at m/z 191 for tri-, tetra- and pentacyclic triterpenes, at m/z 217 for steranes and rearranged steranes, at m/z 253 for monoaromatic steranes, m/z 231 for tri-aromatic steranes, phenanthrene, and methyl-phenanthrene at 178 and 192, dibenzothiophene (DBT) and methyl- DBT at m/z 184 and 198 determined using the record and ion fragmentogram definitions are given in SI table. Elution order matching and retention time were used to identify compounds. The Turkish Petroleum Corporation's Oil and Organic Geochemistry Laboratory (TPAO, Ankara) performed the analyses.

Additionally, vitrinite reflectance (Ro %) values were calculated based on $T_{max}$ (Jarvie *et al.* 2001). The Ro % is calculated using the following formula:

$$Ro\% = (0.018 \times T_{max}) - 7.16 \quad (4)$$

## 4. Results

### 4.a. Lithology

In this investigation, the shale samples were collected from the Lutetian age sequence from the Everek area. Here the sequence starts with sandstones at the base and keeps going with sandstone, marl and shales. The layer thickness of sandstones generally varies between 10 and 100 cm. The layer thicknesses of marl and shales are quite variable and marl layers vary between 4 cm and 50 cm, and shale layers vary between 2 cm and 30 cm. The total thickness of the sequence is 380 m. It starts with brown-grey, thick-layered sandstone (about 1 m thick) and continues for 20 metres (Fig. 2a, b). Throughout to the top, the section is formed of thin-thick-bedded brown-grey sandstone, thick-medium-bedded green-grey marl and medium, thin-bedded grey-dark grey-black shale (Fig. 2c, d). Therefore, while sandstone dominates in the lower parts of the stratigraphic section, shale and marl become dominant towards the top. The shales show a dark grey to black colour, especially in the central parts of the sequence, and are usually laminated. Intra-layer sedimentary structures (lamination and gradation), and sub-layer sedimentary structures (flute, load and rill marks) have been detected in the section and many remarkably well-preserved plant fragments (Fig. 2e). These sedimentary structures are the primary indicators of sequences transported and deposited by turbidity currents. It is possible to classify these turbidity currents into two groups: a) hyperpycnal turbidites and low-density turbidites (Gani, 2004; Mutti *et al.* 2009; Yang *et al.* 2015; Zhang *et al.* 2021). Hyperpycnal turbidity currents are high-density flows that carry high concentrations of sediment particles; they are observed at the bottom of the section. Because coarse-grained and thick-layered sandstones are more dominant in the lower part of the section than in the upper part, an upward-fining grain sequence is observed above the higher energy deposits; this corresponds to the energy attenuation zone with limited erosion capacity. Moderate, low-density flows have a low erosional capacity and mostly form fining-upward sequences, as observed at the top and medium of the section, respectively. These flows can erode, and ripples are produced by bedload reworking and low-amplitude bed waves. In this study, low-density turbidites contain higher amounts of TOC than hyperpycnal turbidites.

### 4.b. Major and trace elements

Trace and major element concentrations of the studied black shale are listed in Table 1. Trace and major elements protect a wealth of palaeo-redox and palaeo-climate knowledge beneficial to the reconstruction of the early diagenetic history and depositional environment of fine-grained detrital rocks (Wu *et al.* 2021; Li *et al.* 2020; Lin *et al.* 2019; Zhang *et al.* 2018).

$SiO_2$ and $Al_2O_3$ contents of the black shale range from 48.83 to 53.30 wt% (mean 51.36 wt%) and 14.73 to 17.52 wt% (mean 15.90 wt%), respectively. $Fe_2O_3$ content of the samples is extremely similar to one another and varies between 8.09 and 8.51 wt% (mean 8.29 wt%). MgO, CaO and $K_2O$ contents of the samples range from 4.36 to 5.45 wt% (mean 4.90 wt%), 2.09 to 5.26 wt% (mean 4.01 wt %) and 1.87 to 2.87 wt% (mean 2.48 wt%), respectively. Other major element oxides such as $TiO_2$, $Na_2O$, MnO, $P_2O_5$ and $Cr_2O_3$ have low contents, those of $Na_2O$ and $TiO_2$ are higher than 1 wt%, and others are less than 1 wt% (Table 1). The mean concentrations of the chosen trace element in the samples indicate the following trends Ba (306ppm) > V (191ppm) > Ni (175ppm) > Sr(151ppm) > Cu (62.8ppm) > Co (36.5 ppm) > Th (28.0 ppm) > Zn (22.2 ppm) > U (1.93 ppm) > Mo (0.33 ppm) > Cd(0.20 ppm) (Table 1).

The ratios of Th/U, C-values and CIA values used as palaeo-climate indicators vary from 3.63 to 4.76, 0.64 to 1.12 and 42 to 62 (Table 2), respectively. The ratios of Cu/Zn, Ni/Co and V/(V+Ni) used as palaeo-redox indicators range from 2.10 to 2.48, 4.14 to 5.42 and 0.51 to 0.56, (Table 2), respectively. The ratios of Sr/Ba and TS/TOC used as palaeo-salinity indicators vary from 0.35–0.65 to 0.07–0.49 (Table 2), respectively. The ratios of Ni/Al, Cu/Al and Zn/Al utilized as palaeo-productivity indicators are between 0.019 and 0.022, 0.006 and 0.007 and 0.002–0.003, respectively. The ratio

https://doi.org/10.1017/S0016756824000281 Published online by Cambridge University Press

**Table 1.** Concentrations of elements in the analyzed groups of black shale

| Sample no | $SiO_2$ | $Al_2O_3$ | $Fe_2O_3$ | MgO | CaO | $Na_2O$ | $K_2O$ | $TiO_2$ | $P_2O_5$ | MnO | $Cr_2O_3$ |
|---|---|---|---|---|---|---|---|---|---|---|---|
| | | | | | | % | | | | | |
| E-3 | 49.03 | 16.75 | 8.33 | 5.23 | 4.56 | 1.79 | 2.87 | 1.08 | 0.14 | 0.08 | 0.040 |
| E-7 | 48.83 | 16.95 | 8.51 | 5.27 | 4.47 | 1.34 | 2.73 | 1.13 | 0.14 | 0.08 | 0.039 |
| E-13 | 52.68 | 14.82 | 8.26 | 4.36 | 4.84 | 2.19 | 1.87 | 0.92 | 0.17 | 0.07 | 0.027 |
| E-15 | 50.78 | 15.23 | 8.1 | 4.45 | 4.77 | 1.89 | 2.63 | 1.32 | 0.17 | 0.07 | 0.032 |
| E-16 | 50.71 | 14.73 | 8.18 | 4.66 | 5.26 | 1.64 | 2.19 | 1.09 | 0.16 | 0.08 | 0.037 |
| E-17 | 53.30 | 16.45 | 8.18 | 4.99 | 2.43 | 1.84 | 2.53 | 1.05 | 0.15 | 0.07 | 0.036 |
| E-20 | 51.56 | 15.78 | 8.12 | 5.07 | 3.43 | 1.73 | 2.62 | 1.12 | 0.16 | 0.08 | 0.029 |
| E-22 | 51.89 | 15.87 | 8.09 | 5.11 | 3.93 | 1.56 | 2.54 | 0.98 | 0.16 | 0.07 | 0.038 |
| E-24 | 53.11 | 14.88 | 8.32 | 4.45 | 4.32 | 1.48 | 1.99 | 1.73 | 0.14 | 0.08 | 0.028 |
| E-26 | 51.69 | 17.52 | 8.80 | 5.45 | 2.09 | 1.61 | 2.84 | 1.18 | 0.15 | 0.08 | 0.041 |
| Mean | 51.36 | 15.90 | 8.29 | 4.90 | 4.01 | 1.71 | 2.48 | 1.16 | 0.15 | 0.08 | 0.030 |
| | Sr | Cu | Ba | Th | U | V | Ni | Zn | Co | Cd | Mo |
| | | | | | | ppm | | | | | |
| E-3 | 117.3 | 69.7 | 281 | 7.9 | 2 | 201 | 194 | 87 | 38.6 | 0.20 | 0.20 |
| E-7 | 112.8 | 68.4 | 279 | 8.6 | 2.1 | 207 | 200 | 83 | 40.0 | 0.20 | 0.10 |
| E-13 | 203.3 | 50.0 | 320 | 6.9 | 1.9 | 160 | 148 | 89 | 27.3 | 0.30 | 0.60 |
| E-15 | 157.6 | 56.9 | 289 | 8.3 | 1.8 | 196 | 157 | 92 | 37.9 | 0.20 | 0.30 |
| E-16 | 170.6 | 62.0 | 262 | 6.8 | 1.7 | 180 | 175 | 85 | 34.5 | 0.20 | 0.40 |
| E-17 | 168.2 | 61.0 | 351 | 8.1 | 1.7 | 183 | 167 | 98 | 33.4 | 0.20 | 0.30 |
| E-20 | 119.3 | 56.1 | 341 | 8.2 | 2.2 | 203 | 178 | 88 | 35.7 | 0.30 | 0.40 |
| E-22 | 187.2 | 59.4 | 319 | 8.4 | 2.0 | 195 | 182 | 91 | 40.1 | 0.10 | 0.50 |
| E-24 | 148.3 | 71.6 | 298 | 7.5 | 1.6 | 189 | 169 | 84 | 37.5 | 0.20 | 0.40 |
| E-26 | 129.7 | 72.4 | 323 | 9.2 | 2.3 | 192 | 184 | 89 | 39.8 | 0.10 | 0.10 |
| Mean | 151.0 | 62.8 | 306 | 7.99 | 1.93 | 191 | 175 | 89 | 36.5 | 0.20 | 0.33 |

**Table 2.** Concentrations of elemental ratios in the analyzed groups of black shale

| | Palaeo-climate | | | Palaeo-productivity | | | Detrital | Palaeo-redox | | | Palaeo-salinity | |
|---|---|---|---|---|---|---|---|---|---|---|---|---|
| Sample no | Th/U | C-values | CIA | Ni/Al | Cu/Al | Zn/Al | Ti/Al | Cu/Zn | Ni/Co | V/(V+Ni) | Sr/Ba | TS/TOC |
| E-3 | 3.95 | 1.07 | 46 | 0.022 | 0.006 | 0.002 | 0.07 | 2.32 | 5.03 | 0.51 | 0.42 | 0.12 |
| E-7 | 4.10 | 1.12 | 48 | 0.022 | 0.006 | 0.002 | 0.08 | 2.47 | 5.00 | 0.51 | 0.40 | 0.07 |
| E-13 | 3.63 | 0.64 | 43 | 0.019 | 0.006 | 0.003 | 0.07 | 2.10 | 5.42 | 0.52 | 0.64 | 0.29 |
| E-15 | 4.61 | 0.87 | 44 | 0.019 | 0.007 | 0.003 | 0.10 | 2.21 | 4.14 | 0.56 | 0.55 | 0.13 |
| E-16 | 4.00 | 0.89 | 42 | 0.022 | 0.006 | 0.003 | 0.08 | 2.23 | 5.07 | 0.51 | 0.65 | 0.23 |
| E-17 | 4.76 | 0.74 | 58 | 0.019 | 0.006 | 0.003 | 0.07 | 2.14 | 5.00 | 0.52 | 0.48 | 0.47 |
| E-20 | 3.73 | 0.90 | 51 | 0.021 | 0.007 | 0.003 | 0.08 | 2.40 | 4.99 | 0.53 | 0.35 | 0.23 |
| E-22 | 4.20 | 0.82 | 49 | 0.022 | 0.006 | 0.003 | 0.07 | 2.48 | 4.54 | 0.52 | 0.59 | 0.14 |
| E-24 | 4.69 | 0.88 | 46 | 0.021 | 0.007 | 0.003 | 0.13 | 2.23 | 4.51 | 0.53 | 0.50 | 0.49 |
| E-26 | 4.00 | 0.91 | 62 | 0.020 | 0.006 | 0.003 | 0.08 | 2.28 | 4.62 | 0.51 | 0.40 | 0.19 |
| Mean | 4.14 | 0.88 | 49 | 0.021 | 0.006 | 0.003 | 0.08 | 2.28 | 4.83 | 0.52 | 0.50 | 0.24 |

https://doi.org/10.1017/S0016756824000281 Published online by Cambridge University Press

**Table 3.** Rock-Eval and carbon isotope analysis results and calculated parameters

| Sample | TOC (%) | $S_1$(mg/g) | $S_2$(mg/g) | $S_3$(mg/g) | $T_{max}$(°C) | HI | OI | PI | RC (%) | PC (%) | MINC (%) | PP ($S_1$+$S_2$) | Ro (%) | $S_2/S_3$ | BI | TS | $\delta^{13}$Corg |
|---|---|---|---|---|---|---|---|---|---|---|---|---|---|---|---|---|---|
| E-3 | 0.68 | 0.05 | 0.51 | 0.11 | 454 | 75 | 16 | 0.09 | 0.63 | 0.05 | 0.63 | 0.56 | 1.01 | 4.64 | 0.07 | 0.08 | |
| E-7 | 0.69 | 0.05 | 0.52 | 0.11 | 456 | 78 | 16 | 0.09 | 0.63 | 0.06 | 0.47 | 0.57 | 1.05 | 4.73 | 0.07 | 0.05 | |
| E-13 | 0.84 | 0.04 | 0.51 | 0.40 | 455 | 61 | 48 | 0.07 | 0.77 | 0.07 | 0.59 | 0.55 | 1.03 | 1.28 | 0.05 | 0.24 | |
| E-15 | 6.54 | 0.63 | 12.49 | 0.20 | 449 | 191 | 3 | 0.05 | 5.43 | 1.11 | 0.55 | 13.1 | 0.92 | 62.45 | 0.10 | 0.83 | −28.23 |
| E-16 | 2.25 | 0.29 | 2.67 | 0.14 | 453 | 119 | 6 | 0.10 | 1.99 | 0.26 | 0.92 | 2.96 | 0.99 | 19.07 | 0.13 | 0.51 | −28.22 |
| E-17 | 0.86 | 0.05 | 0.72 | 0.13 | 456 | 84 | 15 | 0.06 | 0.79 | 0.07 | 0.37 | 0.77 | 1.05 | 5.54 | 0.06 | 0.4 | |
| E-20 | 0.56 | 0.03 | 0.41 | 0.11 | 456 | 73 | 20 | 0.07 | 0.52 | 0.04 | 0.44 | 0.44 | 1.05 | 3.73 | 0.05 | 0.13 | |
| E-22 | 2.01 | 0.07 | 2.09 | 0.18 | 455 | 104 | 9 | 0.03 | 1.82 | 0.19 | 0.78 | 2.16 | 1.03 | 11.61 | 0.03 | 0.28 | |
| E-24 | 0.63 | 0.04 | 0.46 | 0.09 | 458 | 73 | 14 | 0.09 | 0.58 | 0.05 | 0.25 | 0.50 | 1.08 | 5.11 | 0.06 | 0.31 | |
| E-26 | 0.62 | 0.04 | 0.45 | 0.11 | 457 | 73 | 18 | 0.08 | 0.57 | 0.05 | 0.31 | 0.49 | 1.07 | 4.09 | 0.06 | 0.12 | |
| Mean | 1.57 | 0.13 | 2.08 | 0.16 | 455 | 93 | 17 | 0.07 | 1.37 | 0.20 | 0.53 | 2.21 | 1.03 | 12.22 | 0.08 | 0.30 | |

**Table 4.** The parameters were calculated from gas chromatograms (GC) for selected shale samples

| Örnek No | Pr/Ph | Pr/n-$C_{17}$ | Ph/n-$C_{18}$ | n-$C_{17}$/n-$C_{27}$ | CPI | OEP | TAR | WI |
|---|---|---|---|---|---|---|---|---|
| E-15 | 7.48 | 2.35 | 0.32 | 0.62 | 1.11 | 1.03 | 1.42 | 2.61 |
| E-16 | 5.86 | 4.03 | 0.41 | 0.49 | 1.07 | 1.02 | 1.74 | 3.07 |

CPI = 2 × Σ tek n-$C_{23-29}$/(Σ çift n-$C_{22-28}$ + Σ çift n-$C_{24-30}$);
OEP = (n-$C_{21}$ + 6 × n-$C_{23}$ + n-$C_{25}$)/(4 × n$C_{22}$ + 4 × n-$C_{24}$); WI =Σ n-$C_{21-31}$/Σ n-$C_{15-20}$;
TAR = (n-$C_{27}$ + n-$C_{29}$ + n-$C_{31}$)/(n-$C_{15}$ + n-$C_{17}$ + n-$C_{19}$);
Pr = Pristane; Ph = Phytane.

Ti/Al is used as a detrital input indicator and ranges from 0.07 to 0.13 (Table 2). However, it is known that the trace and major elements in the sediments originate from hydrothermal, authigenic, clastic, hydrogenous and biogenic, origins in mixed proportions (Dymond, 1981; Brumsack, 2006; Xu *et al.* 2012; Tripathy *et al.* 2014; Liang *et al.* 2020). When the element is authigenic, it can be used to investigate palaeo-productivity, palaeo-redox and palaeo-salinity conditions (Tribovillard *et al.* 2006).

### 4.c. $\delta^{13}$Corg isotopes

Because this parameter is used by plant communities for photosynthesis, stable carbon isotopic parameters ($\delta^{13}$C) are used to identify the source of the OM (aquatic vegetation, dissolved OM, particulate OM, algae, microbes and terrestrial vascular plants). (Whiticar, 1996; Lamb *et al.* 2006; Samanta *et al.* 2013; Kumar *et al.* 2021).

The bulk fraction of $\delta^{13}$Corg isotope content of the samples is close to each other, measured as −28.23 for E-15 and −28.22 for E-16 (Table 4).

### 4.d. Bulk organic geochemical characteristics

#### 4.d.1. TS, TOC and Rock-Eval pyrolysis

The consequences of the Rock-Eval pyrolysis, TOC analysis and TS values are given in Table 3. TS values of the studied shale samples vary between 0.05 and 0.83% (mean of 0.30%). The TOC abundance of shale samples from Everek varies considerably, ranging from 0.62 to 6.54 % (mean 1.57 %), and the $S_1$+$S_2$ values range from 0.44 to 13.12 mg/g (mean 2.21 mg/g). The HI indicates a narrow variation in the shale samples, varying from 73 to 192 mgHC/g TOC (mean 93 mgHC/g TOC). The highest TOC, HI and $S_1$+$S_2$ values are observed in the middle part of the section (E-15 sample). In addition, HI, $S_1$+$S_2$ values show a linear relationship with TOC (Fig. 3). $T_{max}$ and Ro values of the samples are high, ranging from 449°C to 458°C (mean 455°C), and 0.91 and 1.08, respectively. $T_{max}$ is similar throughout the section, and unlike TOC, $S_1$+$S_2$ and HI, the lowest value was measured in the E-15 sample (Fig. 3). The production index (PI) and bitumen index of the samples range from,0.03 to 0.09 (mean = 0.07) and 0.03 – 0.13 (mean = 0.08), respectively.

#### 4.d.2. n-alkanes and isoprenoids

For sample E-15, n-alkanes in the range n-$C_{13}$–n-$C_{36}$ are characterized by monomodal distributions, with the maximum peak appearing at n-$C_{25}$ (Fig. 4a), while for E-16, n-alkanes are characterized by monomodal distributions in the range n-$C_{15}$–n-$C_{34}$ and the maximum peak also appears at n-$C_{25}$ (Fig. 4b).

Because they capture the redox conditions during sedimentation and diagenesis as well as the palaeo-environmental conditions of the source rocks, phytane (Ph) and pristane (Pr) are often regarded as the most significant acyclic isoprenoid hydrocarbons (Didyk *et al.* 1978; Chandra *et al.* 1994). In both samples, Pr and Ph are the acyclic isoprenoids record, with Pr being very dominant over Ph (Fig. 4a, b). Therefore, Pr/Ph ratios are calculated as 7.48 for E-15 and 5.86 for E-16 (Table 4). Pr/n-C17 ratios are calculated as 2.35 and 4.03 for E-15 and E-16, respectively, and Ph/n-$C_{18}$ ratios are calculated as 0.32 and 0.41 for E-15 and E-16, respectively. The carbon preference index (CPI, Peters & Moldowan, 1993) and odd-to-even predominance (OEP, Scalan & Smith, 1970) values are calculated as 1.11 and 1.03 for E-15, respectively, and 1.07 and 1.02 for E-16, respectively (Table 4). Terrigenous/aquatic ratio (TAR; Bourbonniere & Meyers, 1996)

https://doi.org/10.1017/S0016756824000281 Published online by Cambridge University Press

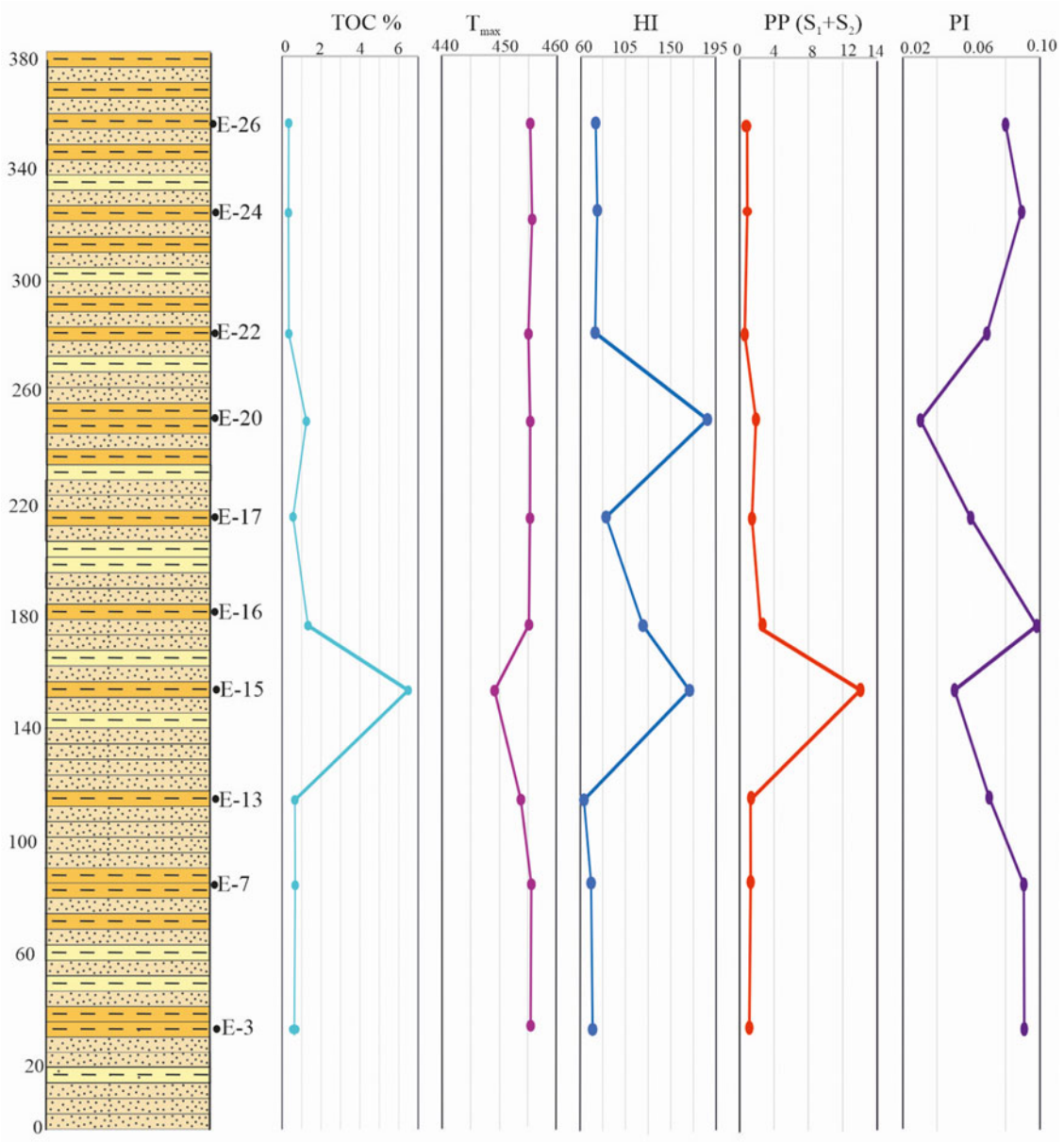


**Figure 3.** (Colour online) Organic geochemical proxy profiles of the black shale samples.

values are higher than 1 and are calculated as 1.42 for E-15 and 1.74 for E-16. The n-$C_{17}$/n-$C_{27}$ ratio represents the marine/aquatic input and is calculated as 0.62 and 0.49 for E-15 and E-16, respectively. The WI values, indicating the contribution of terrestrial plants to the OM (Waxiness index, Peters *et al.* 2005), are calculated as 2.61 and 3.07 for E-15 and E-16, respectively (Table 4).

### *4.d.3. Terpanes and steranes*

Hopanes (pentacyclic terpane), $C_{24}$ Tet (tetracyclic terpane) and $C_{19}$-$C_{26}$ Tri (Tricyclic Terpane) are observed in E-15 and E-16 samples (Fig. 5a, b). The ratios of $C_{19}/C_{23}$ Tri, $C_{24}/C_{23}$ Tri, $C_{26}/C_{25}$ Tri of the E-15 sample are higher than the E-16 sample. The ratios of $C_{19}/C_{23}$ Tri, $C_{24}/C_{23}$ Tri and $C_{26}/C_{25}$ Tri are calculated as 1.02, 0.87 and 1.10 and 0.37, 0.55 and 0.87 for E-15 and E-16 samples, respectively (Table 4). The $C_{24}$Tet/($C_{24}$Tet+ $C_{23}$Tri) ratios of the analyzed samples were close to each other and were calculated as 0.41 and 0.34 for E-15 and E-16, respectively. $C_{29}H/(C_{29}H+C_{29}M)$, $C_{30}H/(C_{30}H+C_{30}M)$ and Ts/(Ts+Tm) ratios are widely used as thermal maturity parameters (Seifert & Moldowan, 1978; George *et al.* 2001). The ratios $C_{29}H/(C_{29}H+C_{29}M)$, $C_{30}H/(C_{30}H+C_{30}M)$and Ts/(Ts+Tm) are calculated as 0.87, 0.87 and 0.23 for E-15, respectively, and 0.91, 0.88 and 0.30 for E-16, respectively. The Gammacerane/$H_{30}$ ratio is utilized to appraise the salinity of the sedimentation environment and the ratios of the Gammacerane/$H_{30}$ of the analyzed samples are highly low and varying from 0.02 to 0.03 for E-15 and E-16, respectively. $C_{31}$22S/22(S+R) ratios are calculated as 0.59 for E-15 and E-16 samples. $C_{32}$22S/22(S+R) ratios for E-15 and E-16 are calculated as 0.58 and 0.60, respectively. While the homohopane index (HHI) was calculated as 0.03 for both samples, the $C_{35}/C_{34}$ ratio was calculated as 0.62 for E-15 and 0.47 for E-16 (Table 4).

https://doi.org/10.1017/S0016756824000281 Published online by Cambridge University Press

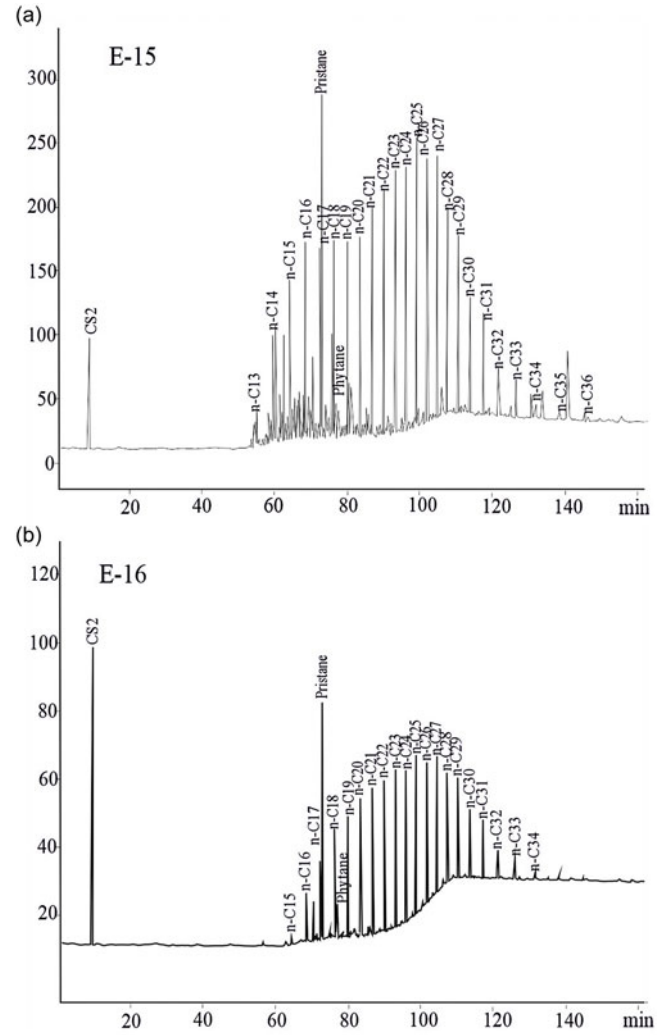


**Figure 4.** Gas chromatograms of saturated hydrocarbons of two representative black shale samples.

The sterane distributions are indicated in Fig. 5 c, d; their concentrations are lower than hopanes with the sterane/hopane ratio calculated as 0.32 for E-15 and 0.20 for E-16 (Table 4). $C_{27}$Dia(Dia+Regular) sterane ratios are calculated as 0.40 for E-15 and 0.70 for E-16. The ααα20Rsteranes are characterized by lower proportions of $C_{27}$ (20 % for E-15 and 20 % for E-16) compared to $C_{28}$ (20 % for E-15 and 24 % for E-16), and $C_{29}$ (60 % for E-15 and 56 % for E-16). The equilibrium point of the $C_{29}$ ββ/(ββ + αα) ratio varies between 0.67 and 0.71 (Seifert & Moldowan 1986). The calculated $C_{29}$ ββ/(ββ + αα) ratios of E-15 and E-16 samples are 0.61 and 0.55, respectively.

#### 4.d.4. Aromatic hydrocarbons

In the m/z 192 and 178 mass chromatograms of the E-15 and E-16 samples, phenanthrene (P) constitutes the dominant peak, and methyl phenanthrene abundances are approximately similar (Fig. 6a, b). While DBT has the highest abundance in the m/z 184-198 mass chromatograms of both samples, methyl dibenzothiophenes (MDBTs) show approximately similar distribution (Fig. 6c, d). In the m/z 231 mass chromatogram of both samples, the highest value belonged to the $C_{28}$ tri-aromatic steroid, while the lowest value was recorded in the $C_{27}$ tri-aromatic steroid (Fig. 6 e, f). The TAI/(TAI+TAII) ratio was calculated as 0.78 for the E-15 sample and 0.80 for the E-16 sample (Table 5). In the m/z 253 mass chromatogram of both samples, while $C_{29}$ monoaromatic steroid has the highest value, the lowest value belongs to $C_{27}$ monoaromatic steroid (Fig. 6g, h). The order is monoaromatic steroid $C_{29} > C_{28} > C_{27}$ (57 %, 27 %, 16 % in the E-15 and 48 %, 26 %, 26 % in the E-16) and the $C_{29}/C_{27}$ ratio is calculated as 3.59 for E-15 and 1.89 for E-16 (Table 4). The MAI/(MAI+MAII) ratio is not very high and is calculated as 0.25 for E-15 and 0.21 for E-16 (Table 4).

## 5. Discussion

### 5.a. Nature of organic matter and deposition environment

To define the OM type of black shale samples, the $S_2/S_3$ ratios (hydrocarbon type index) and hydrogen index (HI) values obtained from TOC and pyrolysis analysis results were used. The HI vs $T_{max}$ diagram developed by Lafargue *et al.* (1998) is widely used to determine the kerogen type. Kerogen type, which is commonly classified under three groups (Type I, II and III), provides very important information about the source from which OM is derived. Type III kerogen is primarily composed of terrestrial plants, Type I kerogen is derived dominantly from alginite and Type II kerogen has a mixed source of marine organisms and higher terrestrial plant debris (Zhou *et al.* 2023).

In the HI vs $T_{max}$ diagram, 7 samples of black shale were in the Type II–III kerogen and oil-gas-prone region, while three samples of shale were in the Type II kerogen and oil-prone region (Fig 7a). $S_2/S_3$ ratios of the analyzed samples are widely distributed and vary between 1.28 and 62.45 (Table 3). According to the classifications of Clementz *et al.* (1979) and Peters & Cassa (1994), the kerogen content of these samples changes between Type III and Type I/Type II, Type III and Type I, respectively. Based on this, we can talk about mixed OM, with OM predominantly coming from terrestrial plants. Additionally, the high value of the correlation coefficient and the linear distribution of the samples in the $S_1$ vs $S_2$ graph ($r = 0.96$, Fig 7b) indicate that a single source is dominant for OM. However, only terrestrial OM is characterized by relatively higher $S_3$ values and lower $S_2/S_3$. The samples in the TOC-$S_2/S_3$ diagram show linear spread in a narrow range (ratios ($r = 0.78$, Fig 7c) (Mallick *et al.* 2022), confirming that a single source is dominant. The fact that the $S_2/S_3$ ratios of all the samples are >1 (1.28 – 62.45) suggests mixed type OM. This shows the limited contribution of marine OM, as well as the intense OM input coming from land during the deposition of shales, which is supported by C isotope values as explained below.

OM obtained from terrestrial vascular C3 plants has $\delta^{13}C$ isotope values ranging from −22 to −33, whereas the $\delta^{13}C$ isotope values of C3 aquatic plants vary between −13 and −27‰ (Whiticar, 1996). $\delta^{13}C$ isotope values of bacteria in coastal and open sea environments vary between −12 and −27‰ depending on their source (Coffin *et al.* 1989). The analyzed samples' $\delta^{13}C$ isotope levels are in the range of values seen in OM obtained from terrestrial vascular C3 plants. In this context, the OM contained in the studied shales is thought to be predominantly of terrestrial origin.

Gas chromatograms of selected samples have low to high-weight n-alkanes and the n-alkanes distribution varies between n-$C_{13}$-n-$C_{36}$ for E-15 and n-$C_{15}$-n-$C_{34}$ for E-16. This distribution reflects a mixture of algae/bacteria (Hunt, 1996) and terrestrial plants (Eglinton & Hamilton, 1967; Killops & Killops, 2005;

https://doi.org/10.1017/S0016756824000281 Published online by Cambridge University Press

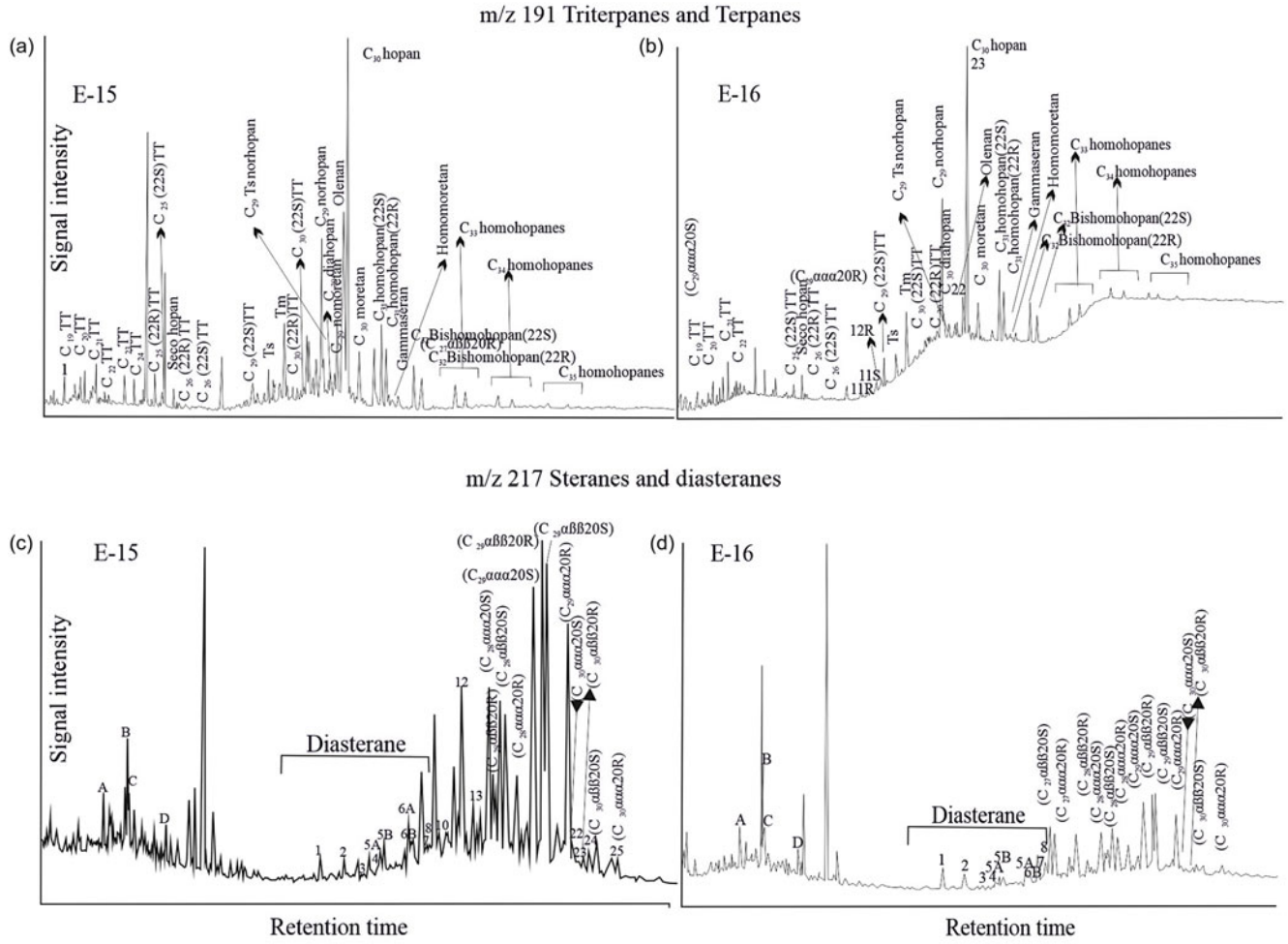


**Figure 5.** The m/z 191 mass fragmentograms (on top) and m/z 217 mas fragmentograms (below) saturated hydrocarbon fractions of two representative black shale samples.

Saydam Eker, 2013; Qiao *et al.* 2021). The high $n$-$C_{17}$/$n$-$C_{27}$ ratio reflects the dominance of marine OM over terrestrial OM. In this study, the $n$-$C_{17}$/$n$-$C_{27}$ ratios are < 1 (vary between 0.62 and 0.49) indicating OM of terrestrial is more predominant. TAR values of the samples are >1, supporting that terrestrial OM is more dominant than marine OM. These values mentioned above reflect the existence of both marine and terrestrial OM in the depositional environment. However, in the Pr/$n$-$C_{17}$ vs. Ph/$n$-$C_{18}$ graph, which is widely used to interpret the origin of OM and the depositional environment, the samples fell into the terrestrial OM area. This can be explained by the high amount of pristane due to the oxic-suboxic environment (Fig. 8).

The primary sources of the biomarker compounds sterane and hopane, respectively, are bacteria and plants/algae (Rohmer & Outrissan 1976). While high amounts of $C_{19}$ and $C_{20}$ TT indicate terrestrial OM (Peters *et al.* 2005), the dominance of $C_{23}$ TT exhibits a reducing marine carbonate environment and marine OM input (Waples & Machihara, 1991; Tao *et al.* 2015; Qiao *et al.* 2021). While the E-15 sample's $C_{19}/C_{23}$ TT ratio is calculated as >1, indicating the dominance of terrestrial OM, the E-16 sample's $C_{19}/C_{23}$ TT ratio is calculated as <1, indicating the dominance of marine OM (Table 4). For this reason, it can be said that there is both marine and terrestrial OM in the depositional environment. The high $C_{24}Tet/(C_{24}Tet+C_{23}TT)$ ratio indicates that OM includes a mixture of aquatic algal-bacterial and terrestrial OM (Alexander *et al.* 1983; Connan *et al.* 1986; Peters *et al.* 2005). The $C_{24}Tet/(C_{24}Tet+C_{23}TT)$ ratio of the analyzed black shale samples is not very low and varies between 0.34 and 0.41 (Table 4), confirming the dominance of terrestrial OM as well as the presence of aquatic algae and bacteria. While $C_{29}$ steranes derive from continental higher plants, $C_{27}$ steranes are generally of algal origin (Huang & Meinschein, 1979; Moldowan *et al.* 1986; Volkman, 2003;). In the studied samples, in order $C_{29}$ααα20R>$C_{28}$ααα20R>$C_{27}$ααα20R is observed (Table 4). In this context, the dominance of $C_{29}$ααα20R steranes over $C_{28}$ααα20R and $C_{27}$ααα20R steranes in the black shale samples indicates the dominance of terrestrial OM (Fig. 9).

Although some phytoplankton and microalgae produce the aromatic component $C_{29}$ sterol, the major origin of this sterol is terrestrial plants (Volkman *et al.* 1999; Volkman, 2003; Kostova *et al.* 2022;). $C_{28}$ sterols are highly high in microalgae of marine (Barrett *et al.* 1995; Volkman *et al.* 1998; Volkman, 2003), while $C_{27}$ sterols are typically derived from marine phytoplankton (Brassell & Eglinton, 1981; Volkman, 1986). Therefore, the $C_{29}/C_{27}$ sterol ratio is accustomed to determining the proportion of terrestrial/phytoplankton OM in the environment. $C_{29}/C_{27}$

https://doi.org/10.1017/S0016756824000281 Published online by Cambridge University Press

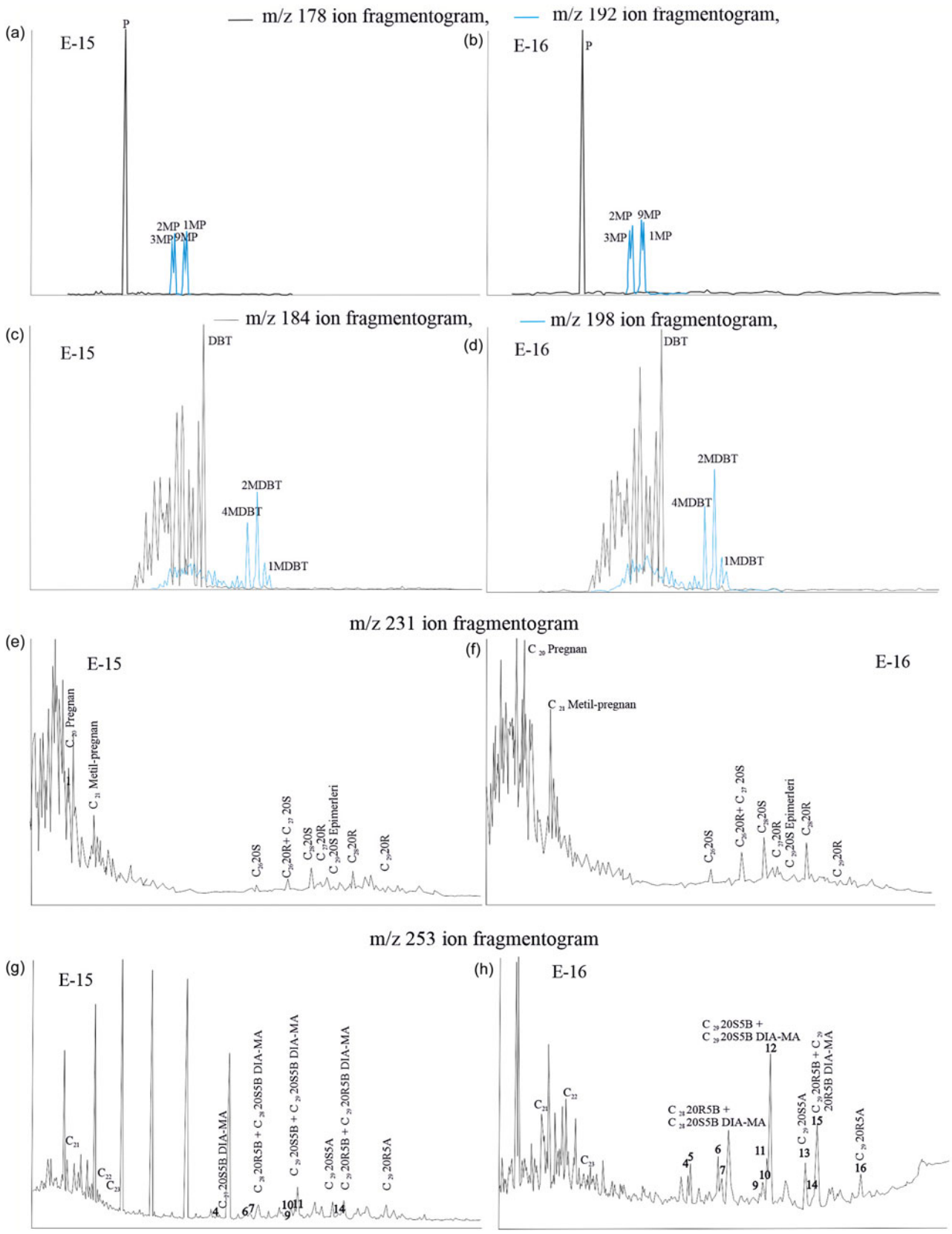


**Figure 6.** (Colour online) The m/z 178-192, m/z 184-198, m/z 231 and m/z 253 ion fragmentograms aromatic hydrocarbon fractions of two representative black shale samples.

https://doi.org/10.1017/S0016756824000281 Published online by Cambridge University Press

**Table 5.** Selected saturated and aromatic biomarker parameters for the selected black shale samples

| Terpane | E-15 | E-16 | Phenanthrene | E-15 | E-16 |
|---|---|---|---|---|---|
| $C_{19}/C_{23}$ Tri. | 1.02 | 0.37 | MPI1 | 0.45 | 0.49 |
| $C_{24}/C_{23}$ Tri. | 0.87 | 0.55 | MPI2 | 0.50 | 0.50 |
| $C_{26}/C_{25}$ Tri. | 1.10 | 0.87 | MPI3 | 0.96 | 0.92 |
| $C_{24}$Tet/($C_{24}$Tet + $C_{23}$ Tri) | 0.41 | 0.34 | MPR | 0.97 | 0.95 |
| Ts/(Ts+Tm) | 0.23 | 0.30 | MPR1 | 0.25 | 0.28 |
| $C_{29}$H/($C_{29}$H+$C_{29}$M) | 0.87 | 0.91 | MPR2 | 0.24 | 0.26 |
| $C_{30}$H/($C_{30}$H+$C_{30}$M) | 0.87 | 0.88 | MPR3 | 0.19 | 0.25 |
| $C_{29}/C_{30}$ hopan | 0.44 | 0.48 | MPR9 | 0.20 | 0.28 |
| $C_{31}$ H22R/$C_{30}$ H | 0.16 | 0.17 | Log(1MP/9MP) | 0.08 | –-0.01 |
| $C_{31}$ H22S/22(S+R) | 0.59 | 0.59 | **Dibenzothiophene** | | |
| $C_{32}$H22S/22(S+R) | 0.58 | 0.60 | DBT/P | 0.11 | 0.11 |
| Gammacerana/$C_{30}$ hopane | 0.02 | 0.03 | MDR | 4.85 | 4.18 |
| Olenan/$C_{30}$ hopane | 0.51 | 0.14 | MDR’ | 0.83 | 0.81 |
| $C_{35}/C_{34}$ HH | 0.62 | 0.47 | | | |
| HHI | 0.03 | 0.03 | **Steroid** | | |
| Sterane/Hopane | 0.32 | 0.20 | TA(I)/TA(I+II) | 0.78 | 0.80 |
| **Sterane** | | | MA(I)/MA(I+II) | 0.25 | 0.21 |
| $C_{27}$Dia/(Dia+Reg) steran | 0.40 | 0.70 | $C_{27.}$ $C_{28.}$ $C_{29}$ MA str. (%) | 16. 27. 57 | 26.26.48 |
| $C_{29}$ααα S/(S+R) sterane | 0.53 | 0.54 | $C_{29}$/ $C_{27}$ | 3.59 | 1.89 |
| $C_{29}$ββ/(ββ+αα) sterane | 0.61 | 0.55 | | | |
| $C_{27.}C_{28.}$ $C_{29}$ ααα sterane (R)(%) | 20, 20, 60 | 20, 24, 56 | | | |

Tri = tricyclic terpanes. Tet = tetracyclic terpanes. H = hopane. M= Moretan. HHI = homohopane index ((HHI. $C_{35}/\Sigma C_{31-35}$ 22S and 22R homohopanes; Peters and Cassa, 1994)). Steranes/hopanes = $C_{27}$-$C_{29}$ regular steranes/$C_{29}$-$C_{35}$ 17α-hopanes. Dia: diasteranes; Reg: regular steranes; Ts: 17α- 22.29.30-trsinorhopane; Tm: 18α-22.29.30-trisnorhopane, MPI= (2MP+3MP)/(1MP+9MP), TAI/(TAI+TAII)= ($C_{20}$+$C_{21}$)/($C_{20}$+$C_{21}$+$C_{26}$+$C_{27}$+$C_{28}$), MA(I)/(MAI+MAII)= ($C_{21}$+$C_{22}$)/($C_{21}$+$C_{22}$+$C_{27}$+$C_{28}$+$C_{29}$).

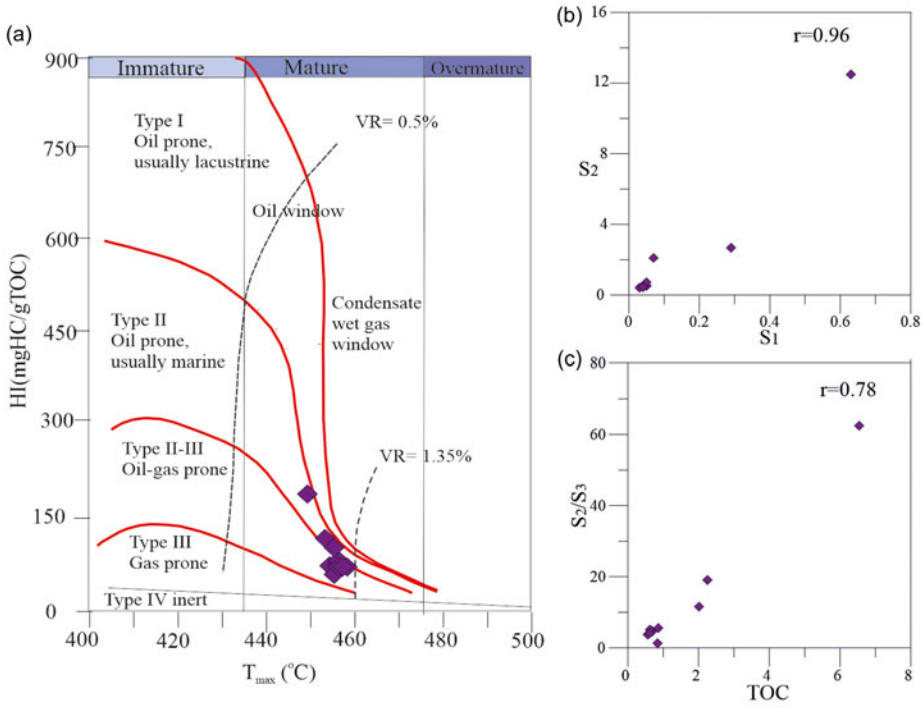


**Figure 7** (Colour online) (a) The plot of $T_{max}$ vs. HI indicates kerogen types for the black shale samples (Lafargue *et al.* 1998), (b) the plot of $S_1$ vs. $S_2$ and (c) TOC vs. $S_2/S_3$ for the black shale samples.

https://doi.org/10.1017/S0016756824000281 Published online by Cambridge University Press

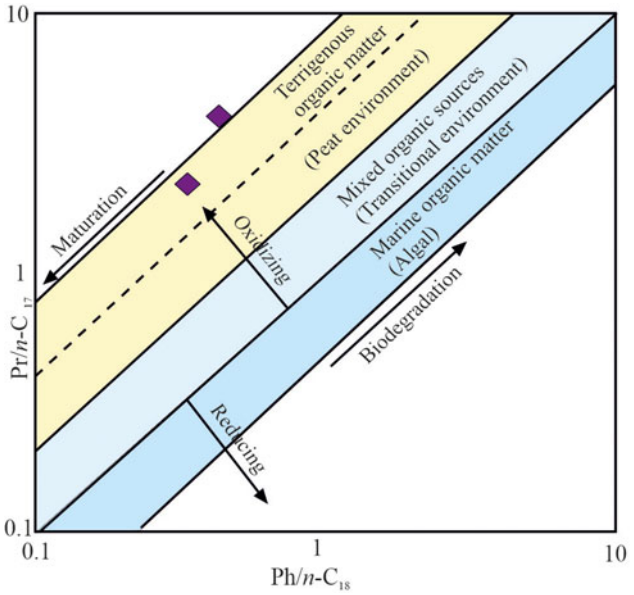


**Figure 8.** (Colour online) The plot of Pr/n-C17 vs. Ph/n-C18 of the black shale samples (Shanmugam, 1985).

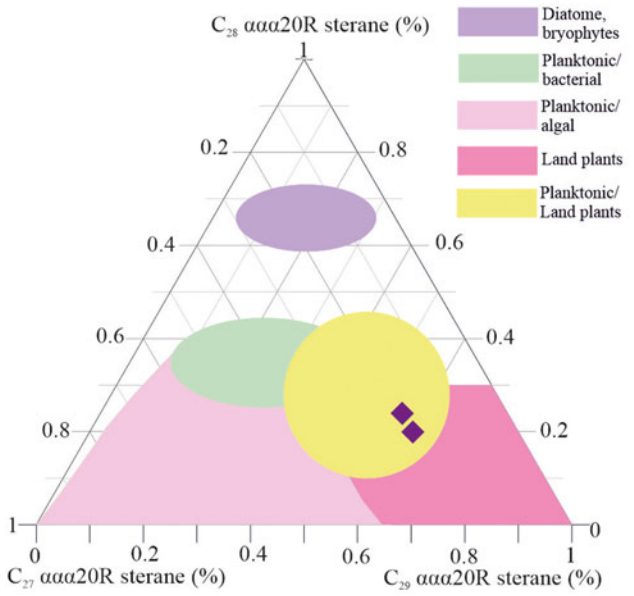


**Figure 9.** (Colour online) The ternary diagram indicating the distribution of $C_{27}$, $C_{28}$, $C_{29}$ ααα 20R steranes (modified from Huang and Meinschein, 1979, after Qiao *et al.* 2021).

sterol < 1 indicates that phytoplankton/algal input is more dominant in the sedimentation environment. The $C_{29}/C_{27}$ ratio of the studied black shale samples is > 1, indicating the dominance of terrestrial OM in the depositional environment. However, $C_{29}$ sterols are represented by stigmastanol (a chemical compound found in many plants) rather than sitosterol (one of the phytosterols whose chemical structure is like cholesterol), which means that plenty of even-numbered n-alkanes are observed over low-weight n-alkanes in anaerobic environments (Welte & Ebhardt, 1968; Welte &Waples, 1973). In this context, it should be kept in mind that a high $C_{29}/C_{27}$ ratio indicates not only the dominance of terrestrial plants but also the presence of aquatic plants, especially in anoxic environments. In the study, it is thought that the depositional environment was oxic-suboxic and the high $C_{29}/C_{27}$ ratio represents terrestrial OM, and the order $C_{29}$MA> $C_{28}$MA>$C_{27}$MA also supports this.

### 5.b. Palaeo-climate

Th/U ratios and C-values are widely used to interpret palaeo-climatic conditions. Cao *et al.* (2012) suggested that Mn, Fe, Cr, Co, Ni and V are relatively enriched under humid conditions. Contrarily, Ca, Mg, K, Na, Sr and Ba are relatively enriched under arid conditions. Warm, humid climates are indicated by Th/U ratios less than 4, whereas hot, dry climates are indicated by higher values (Xu *et al.* 2015; Zhang *et al.* 2021). Low CIA values (70–50) show weak chemical weathering under arid climates, medium CIA values (80–70) reflect moderate chemical weathering under humid and warm climates and high CIA values (100–80) indicate hard chemical weathering under humid and hot climates (Yan *et al.* 2010).

In this study, while the C-values are low (mean of 0.88), the Th/U ratios are generally higher than 4 (mean of 4.14), indicating that the palaeo-climate was arid and hot. The low CIA values of the studied samples indicate that chemical weathering is weak, and the region has an arid and hot climate. The highest CIA value was calculated in sample E-26 (at the top of the MSS), and the lowest CIA value was calculated in E-16 (in the middle of the MSS) (Table 2, Fig. 10).

### 5.c. Palaeo-productivity and detrital influx

Although some researchers (Goldberg & Arrhenius, 1958; Dehairs *et al.* 1980; Dymond *et al.* 1992; McManus *et al.* 1999; Cardinal *et al.* 2005) have noted a clear relationship between Ba and OM abundance, the biogenic contraption of Ba is thought to be some contentious (Liang *et al.* 2020). In this study, the negative relationship between Ba and TOC and the lack of any correlation with Al made the source of the Ba uncertain, therefore, the Ba was not used as a productivity proxy. The elements Cu, Ni and Zn in sediments react with OM (which is usually present in living things) to form complexes that eventually lead them to precipitate at the bottom of the water (Martin and Knauer, 1973; Piper and Perkins, 2004). Therefore, Zn, Cu and Ni were considered proxy productivity indicators due to their micronutrient behaviour (Brumsack, 2006). During deposition, element ratios like Zn/Al, Ni/Al and Cu/Al are commonly employed to assess the palaeo-productivity of source rocks. Increased Ni/Al, Zn/Al and Cu/Al ratios signify higher palaeo-productivity (Algeo and Maynard, 2004; Schoepfer *et al.* 2015; Shen *et al.* 2015)

In this study, Cu/Al, Ni/Al and Zn/Al are quite low, indicating that the productivity is not high. It is known that an arid climate decreases primary productivity, whereas a humid and warm climate increases primary productivity (Meng *et al.* 2012). This means that there is a definite relationship between climate and productivity. During the deposition of the shale, arid and hot climatic conditions existed in the study area, resulting in low productivity.

It is thought that Ti and Al serve as proxies for the input of detrital material (Hatch & Leventhal, 1992; Canfield, 1994; Algeo & Maynard, 2004; Wu *et al.* 2021). Al is mainly found in aluminosilicate minerals such as feldspar and clay (Rimmer, 2004), while titanium often exists in heavy minerals and clays (Kidder *et al.* 2001). As a result, the Ti/Al ratio indicates the energy

https://doi.org/10.1017/S0016756824000281 Published online by Cambridge University Press

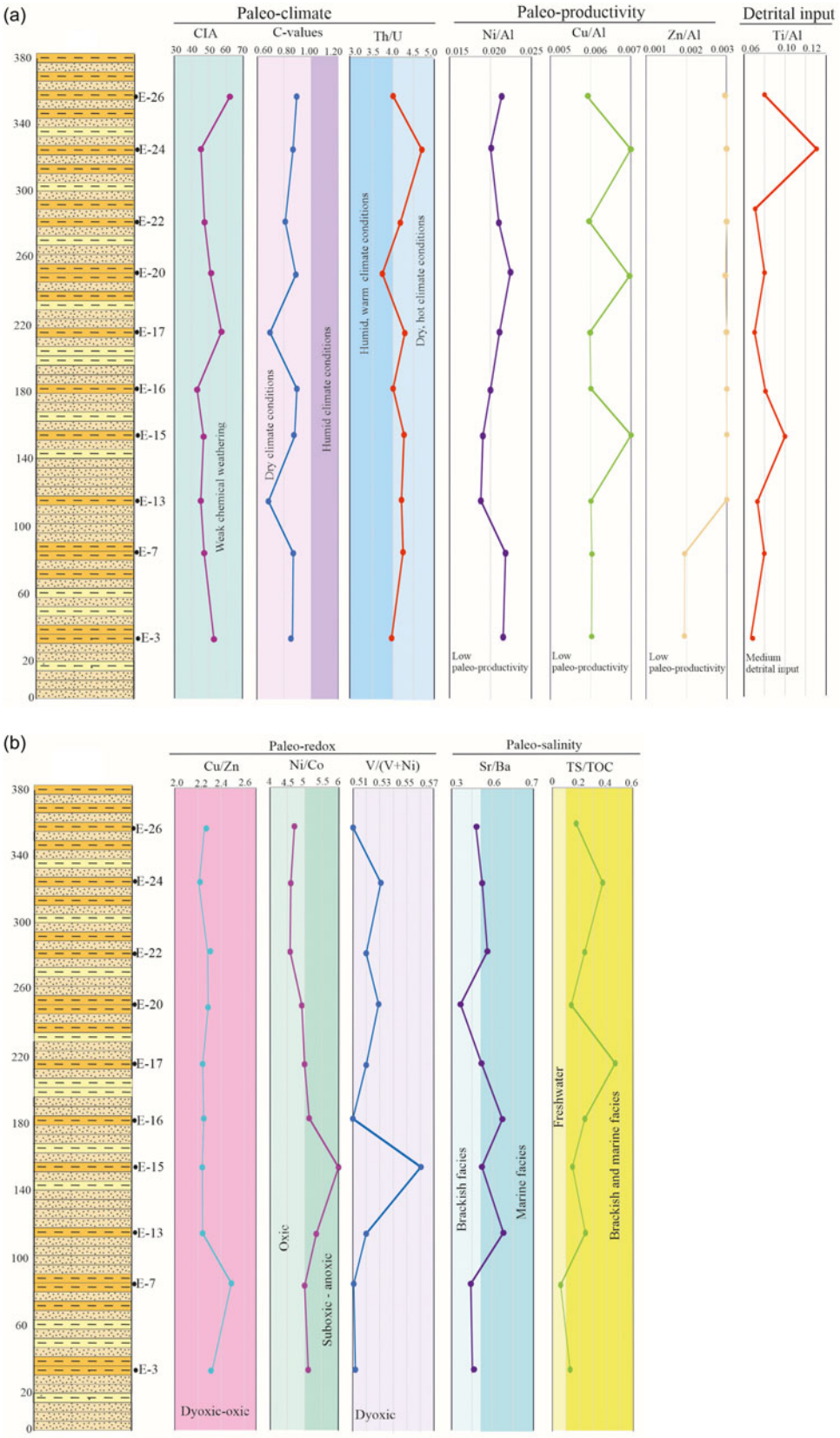


**Figure 10** (Colour online) (a), (b). Inorganic geochemical and proxy profiles of the black shale samples.

https://doi.org/10.1017/S0016756824000281 Published online by Cambridge University Press

of sediment deposition, and Ti and Al abundances aid in identifying the provenance of sediment (Murphy *et al.* 2000; Liang *et al.* 2018; Wu *et al.* 2021).

The Ti/Al ratio of the samples varies between 0.07 and 0.13, and the mean is calculated as 0.08 (Table 2). This value is considered moderate and indicates a medium-energy flow of clastic sediment, representing moderate terrestrial detrital input during this period. Consequently, the OM enrichment was not significantly affected by the dilution of OM caused by detritus sediment influx, as shown by the low correlation relationship between TOC and Ti/Al (r = 0.227).

### 5.d. Palaeo-redox condition

Redox conditions play a significant role in the preservation of OM in the sedimentation environment. The accumulations of some trace elements (e.g. V, U, Cr, Cu, Ni, Zn and Co) express the palaeo-redox conditions (McKay *et al.* 2007). Cu/Zn, Ni/Co and V/V+Ni ratios are commonly used to interpret palaeo-redox conditions. In a sedimentary environment, the Ni/Co ratios above 5 show suboxic and anoxic conditions, while the Cu/Zn values below 5 show oxic conditions (Jones and Manning, 1994; Liang *et al.* 2020). In this study, the Ni/Co ratios of six samples are above 5, the others are below 5, while the Cu/Zn ratios of all samples are below 5 with an average of 2.29, indicating oxic to dysoxic and oxic conditions (Table 2, Fig. 10). Redox conditions classed as euxinic, suboxic to anoxic, dysoxic and oxic are shown by V/(V + Ni) ratios of >0.82, >0.60 to ≤0.82, >0.46 to ≤0.60 and ≤0.46, respectively (Hatch & Leventhal, 1992; Jones & Manning, 1994). V/(V+Ni) ratios of black shale samples are above 0.46 and below 0.60 (mean of 0.52), indicating dysoxic conditions. This determination is also supported by the TS vs V/(V+Ni) diagram. In the diagram, all the samples are in suboxic conditions and a mixture of marine-terrestrial areas (Fig.11).

In addition, Pr/Ph ratios were used to interpret redox conditions in this study. Phytane (Ph) and pristane (Pr) are considered the foremost significant isoprenoid compounds of hydrocarbons in that they indicate the palaeo-environmental conditions of the source rocks and reflect the redox conditions during diagenesis and sedimentation. (Powell & McKirdy, 1973; Didyk *et al.* 1978; Chandra *et al.* 1994; Hakimi and Abdullah, 2014). A high Pr/Ph ratio indicates that the deposition environment is oxic throughout the sedimentation of OM (Mello & Maxwell, 1990; Philp, 1994; Huang *et al.* 2003; Saydam Eker *et al*, 2016b). Peters & Moldowan (1993) stated that Pr/Ph ratio <0.5 reflects a strongly anoxic environment, 0.5<Pr/Ph<1 exhibits an anoxic environment (aquatic), 1<Pr/Ph<2 reflects a weakly oxic-weakly anoxic aquatic environment and Pr/Ph>2 shows an oxic environment. The Pr/Ph ratios of the analyzed black shales are much higher than 2 (Table 4), indicating an oxic condition. A high $C_{35}$ homohopane value is one of the most important indicators of evaporitic and anoxic environments (Boon *et al.* 1983; Connan *et al.* 1986), so the $C_{35}/C_{34}$ homohopane ratio is accustomed to interpreting the redox conditions of depositional environments, and low ratios (< 1) show oxic-dysoxic conditions for the source rock (Curiale *et al.* 1985). The $C_{35}/C_{34}$ HH ratios were calculated as < 1 for the analyzed samples, indicating that the depositional environment was oxic-dysoxic. In addition, low HHI values indicate oxic and/or sulphate-poor, as well as clastic depositional environments (Köster *et al.* 1997; Peters *et al.* 2005).

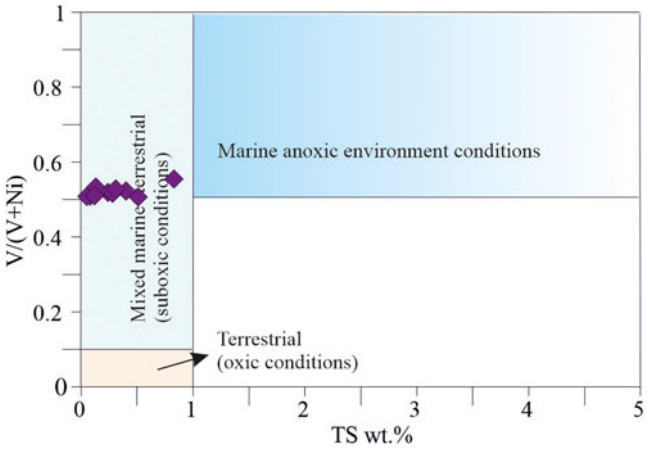


**Figure 11.** (Colour online) Cross-plot of sulphur (TS) and V/(V+Ni) ratio, indicating highly marine reducing environmental conditions black shale samples (Bechtel *et al.* 2001).

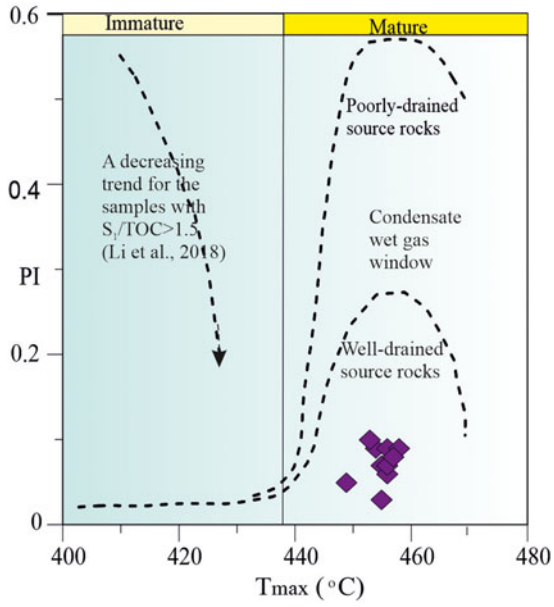


**Figure 12.** (Colour online) The plot of $T_{max}$ vs. PI shows hydrocarbon potential for the black shale samples.

The HHI value of samples E-15 and E-16 was calculated as 0.03, which is low and supports that the deposition environment was oxic and/or sulphate-poor.

### 5.e. Palaeo-salinity

Various parameters (Sr/Ba and TS/TOC ratios) were used to interpret the palaeo-salinity conditions of the depositional environment (e.g. Deng & Qian, 1993; Wei & Algeo, 2020; Zhang *et al.* 2021). S is preserved in the sediment through evaporation, microbial sulphate and thermochemical sulphate reduction (Trundinger *et al.* 1985; Sim *et al.* 2011), thus providing information about the salinity of the environment. TS/TOC is less than 0.1 in freshwater and greater than 0.1 in marine and brackish

https://doi.org/10.1017/S0016756824000281 Published online by Cambridge University Press

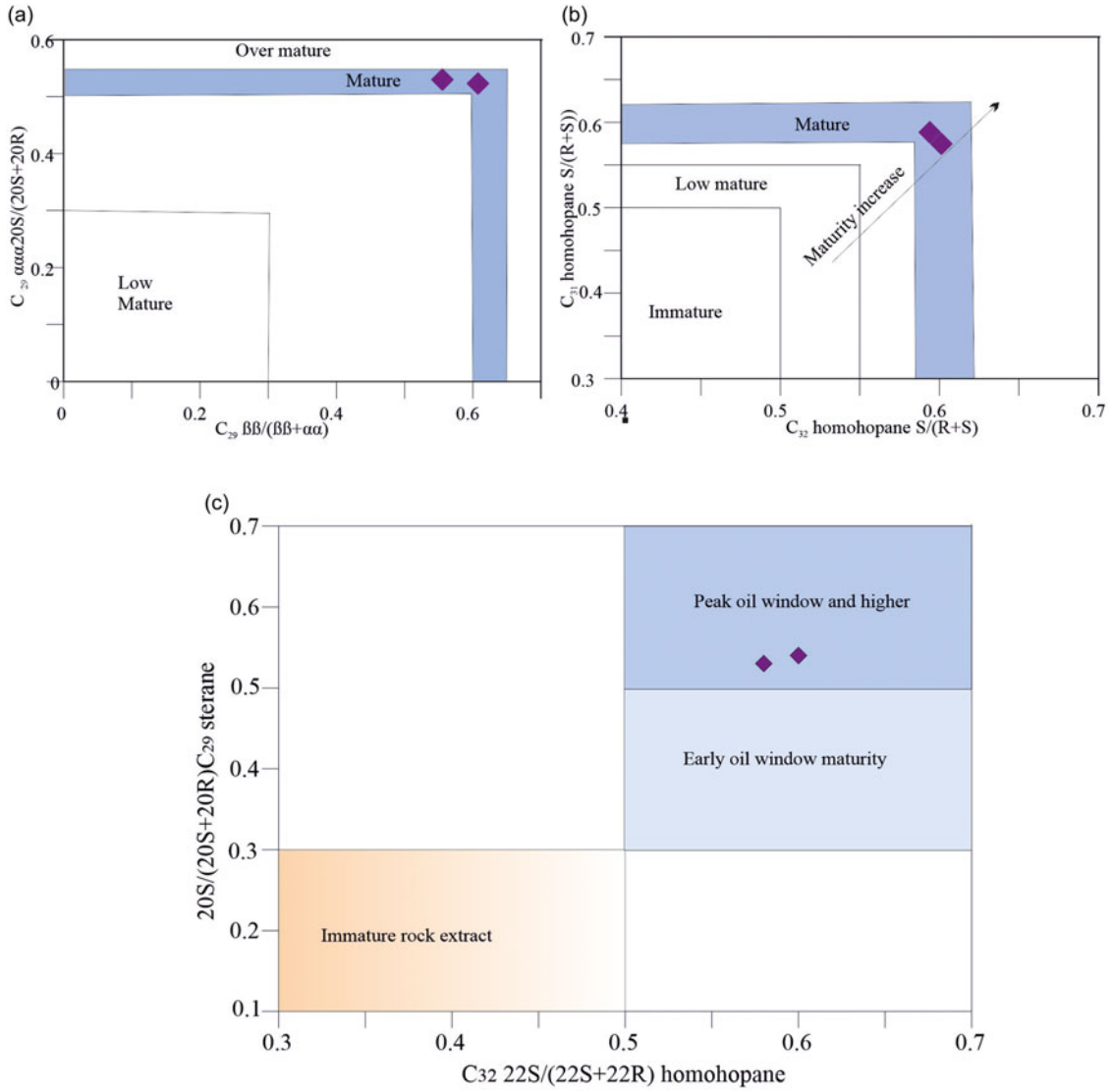


**Figure 13.** (Colour online) The plots of biomarker parameters sensitive to the thermal maturity of the two black shale samples a) (a) $C_{29}$ ααα 20S/(20S + 20R) vs. $C_{29}$ ββ/(ββ + αα), (b) $C_{31}$ homohopan S/(S+R) vs. $C_{32}$ homohopan S/(S+R), (George *et al.* 2001), c)20S(20S+20R) $C_{29}$ sterane vs. $C_{32}$ 22S(22S+22R) homohopane (modified from Peters and Cassa, 1994, from Hakimi & Abdullah, 2014).

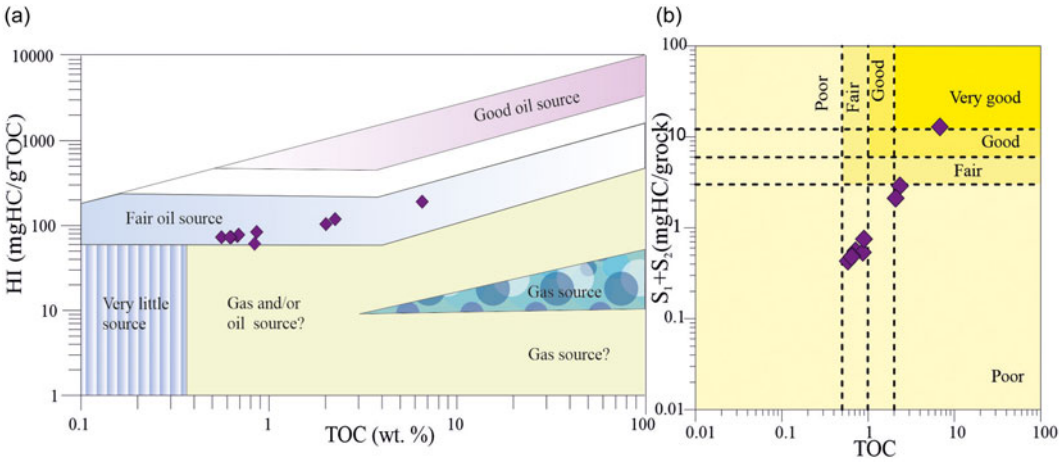


**Figure 14.** (Colour online) The plots of (a) TOC vs. HI (Zhang *et al.*, 2021) and (b) TOC vs $S_1$+$S_2$ (Kostova *et al.* 2022) show source rock characteristics for the black shale samples.

https://doi.org/10.1017/S0016756824000281 Published online by Cambridge University Press

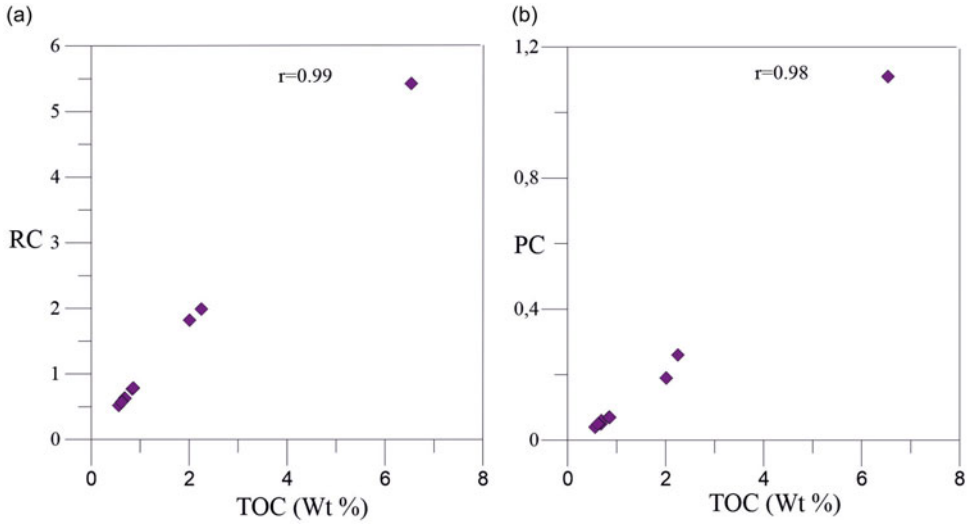


**Figure 15.** (Colour online) The plots of (a) TOC vs. RC and (b) TOC vs. PC show hydrocarbon potential for the black shale samples.

facies. Whereas Sr/Ba is >0.5 in marine facies, it is <0.2 in freshwater and 0.2–0.5 in brackish (Wei & Algeo, 2020). In analyzed shale, the Sr/Ba ratios vary from 0.35 to 0.65 (Table 2, Fig. 10), indicating brackish and marine facies and this finding is also supported by the TS/TOC ratio. TS/TOC ratios vary from 0.07 to 0.49, indicating freshwater and brackish and marine facies and deposition environments.

Gammacerane obtained from biomarker analysis also provides useful information about the palaeo-deposition environment. Gammacerane is generally abundant in high-salt marine environments. In addition, the high gammacerane/$C_{30}$hopane ratio indicates marine depositional environments with high salinity associated with evaporite and carbonate deposition (Peters & Moldowan; 1991). In this study, the gammacerane/$C_{30}$hopane ratios are low, varying between 0.02 and 0.03, indicating a moderate salinity environment.

### 5.f. Thermal maturity of organic matter

The characteristics that are most frequently utilized in thermal maturity studies include the colour change of the palynomorph, vitrinite reflectance and $T_{max}$, which is obtained by programmed temperature pyrolysis (e.g. Hartkopf-Fröder *et al.* 2015; Sorci *et al.* 2020; Spina *et al.* 2021; Buratti *et al.* 2024). In the present study, to determine the OM's thermal maturity, $T_{max}$ and vitrinite reflectance (Ro%) values calculated based on $T_{max}$ (Jarvie *et al.* 2001), aliphatic and aromatic components are used. Aliphatic maturity parameters contain the ββ/(ββ + αα) sterane (reaching an equilibrium value is 0.70), 20S/(20R + 20S) homohopane (value of achieving equilibrium for $C_{29}$ is 0.55) (Seifert & Moldowan, 1986), and 22S/(22R + 22S) homohopane ($C_{32}$), and their ratios increase as maturity increases. Likewise, the 22S/(22R + 22S) homohopane ratios are quite reliable in indicating the thermally early mature to immature range (value ranges from 0.55 to 0.60, Waples & Machihara, 1991; Peters *et al.* 2005). In aromatic components, methyl-DBT ratio and methyl-phenanthrene index (MPI) (MDR = 4MDBT/1MDBT) (Radke & Willsch, 1994) are used as maturity parameters and these rates increase as maturity increases. Additionally, Radke (1987) divided source rock maturity into three groups according to MPI-3 value; MPI-3 > 1 mature, MPI-3 = 0.80–1 medium mature and MPI-3< 0.80 immature.

The $T_{max}$ value of the studied shale samples was measured as > 435 °C and the Ro values were calculated as > 0.70, therefore, the samples of black shale are thermally mature according to the classifications of Mukhopadhyay *et al.* (1995), Espitalié *et al.* (1977) and Peters and Cassa (1994) (Schito *et al.* 2017; Riboulleau *et al.* 2018). The $T_{max}$–PI diagram (Lafargue *et al.* (1998) also supports this; in this graph, all the black shale samples are clustered in the mature area (Fig 12). In the ββ/(ββ + αα) $C_{29}$ sterane and ααα20S/(20S+20R) $C_{29}$ sterane and $C_{32}$ homohopane 22S/(22S + 22R) and $C_{31}$ homohopane 22S/(22S+22R) diagrams, samples E-15 and E-16 have reached the equilibrium value and are therefore thermally mature (Fig. 13a, b). In addition, in the diagram of 20S/(20S+20R) $C_{29}$ sterane and $C_{32}$ 22S/(22S + 22R) homohopane, both samples were collected with peak oil window maturity area (Fig. 13c). However, MPI-3 values of E-15 and E-16 samples were calculated as 4.85 and 4.18, respectively, and MDR ratios were calculated as 0.96 and 0.92, indicating medium thermal maturity. In short, various aromatic indicators exhibit slight differences, but all values ($T_{max}$, Ro %, aliphatic indicators) indicate oil window maturity.

The studied black shales are Lutetian in age and no younger formations were deposited on them in the study area. Therefore, such a high level of thermal maturation cannot be explained by the burial history. It is known that there were volcanic activities near the study area, contemporary with sedimentation during the Eocene (Keskin *et al.* 1990). These volcanic (andesitic, basaltic and pyroclastic rocks) and intrusive rocks (granodiorite, diorite and tonalite) (Kaygusuz & Öztürk, 2015; Eyuboğlu *et al.* 2017; Gücer, 2021) are thought to help increase the temperature of the basin where the black shales were deposited and cause the thermal maturation of the OM.

### 5.g. Source rocks characteristics and hydrocarbon production potential

Regarding low to moderate HI values and TOC contents, the samples can be featured as fair oil source rocks (Fig. 14a). Potential production (PP = $S_1 + S_2$) < 2 mg/HC rock value indicates that the rocks do not have source rock potential, 2-6 mg/HC rock value indicates that the rocks have moderate source rock and hydrocarbon production potential and > 6 mg/HC rock value indicates

https://doi.org/10.1017/S0016756824000281 Published online by Cambridge University Press

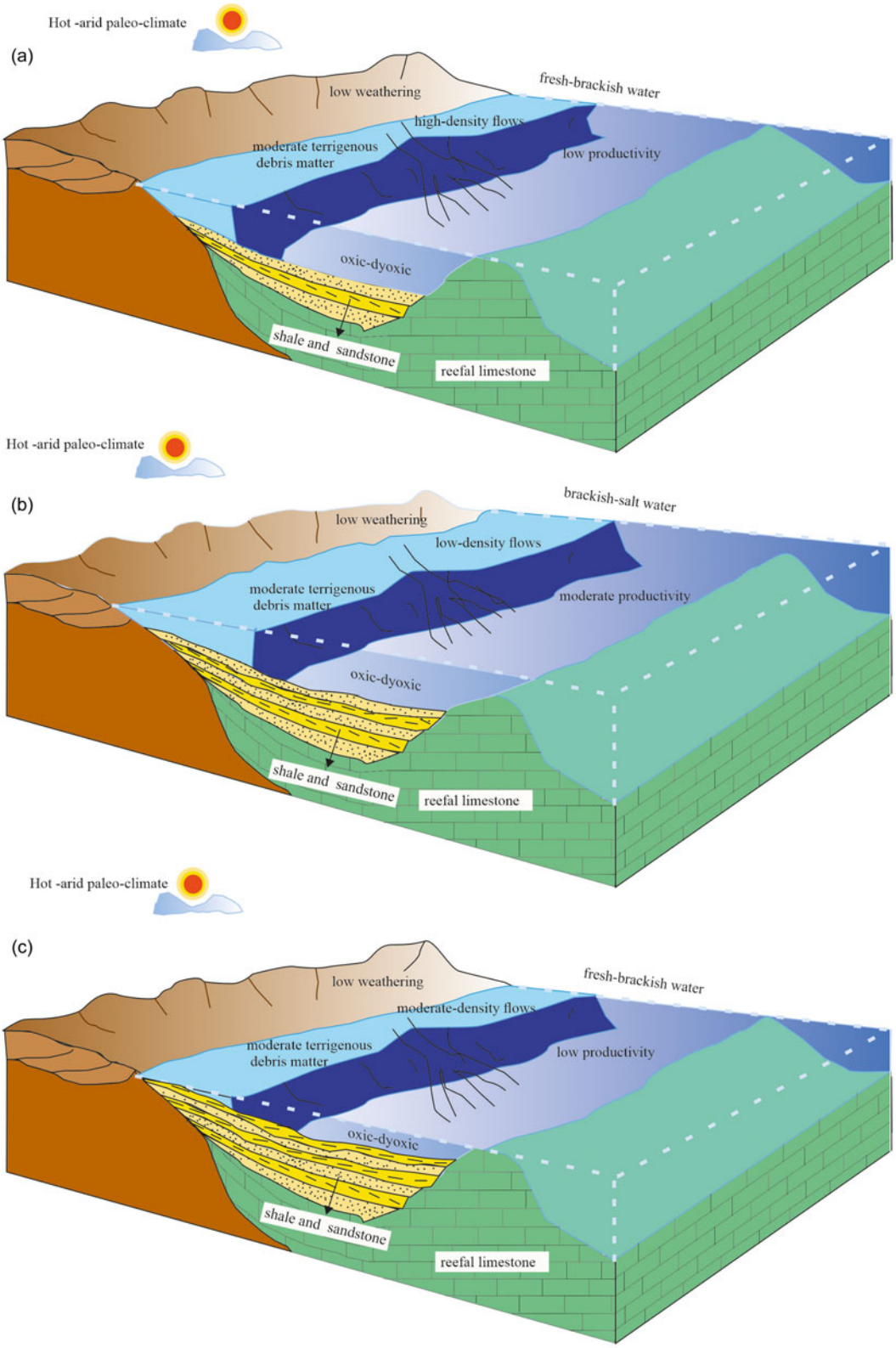


**Figure 16.** (Colour online) Schematic figure showing the organic matter accumulation and sedimentation model of Lutetian clastic rocks, (a) stage I, (b) stage II, (c), stage III.

that the rocks have good source rock and hydrocarbon production potential (Tissot & Welte, 1984). The PP value of one (E-15) of the shale samples is >6 mg/HC rock, the PP value of two (E-16 and E-20) of them varies between 2 and 6 mg/HC rock and the PP value of the others is <2 mg/HC rock. Therefore, the studied shale samples vary from poor to very good source rock, and Figure 14b supports this.

All the studied samples in the $T_{max}$ and PI diagram (Lafargue *et al.* 1998) are in the "well-drained source rock" area (Fig. 12). Hunt (1995) stated that 1% TOC is required for oil production and

https://doi.org/10.1017/S0016756824000281 Published online by Cambridge University Press

0.5% TOC for gas production. TOC values of the samples examined show a very strong positive correlation with RC values (r = 0.99, Fig. 15a), and RC values of 3 samples (E-15, 16 and 20) are > 1%, indicating a few generative potentials left. Furthermore, given the positive relationship between TOC and PC values (r = 0.98, Fig. 15b), thermal maturity and mixed kerogen type (mostly terrestrial and marine), some samples with high TOC content may release little hydrocarbons (English *et al.* 2004; Mallick *et al.* 2022).

In summary, it is observed that primary productivity is generally low in the basin (except in some places) and, accordingly, the amount of OM is not very high. It appears that palaeo-conditions were not suitable for OM accumulation at the top and bottom of the sequence. Conversely, OM-rich shales were deposited in the middle part of the sequence, particularly between 150th and 280th metres. This can be explained by the variability of sea water level, OM productivity, palaeo-salinity, palaeo-redox, palaeo-climatic conditions and terrigenous material input in the basin. However, the palaeo-productivity, palaeo-climate conditions and terrigenous material input amounts of the samples taken from the bottom, middle and top parts of the section are generally similar (Table 2, Fig. 10a). The palaeo-redox and palaeo-salinity conditions of the middle part of the section differ slightly from the bottom and top parts and are relatively higher (Fig. 10b). Therefore, it may be said that the OM enrichments in the Lutetian shales were controlled by palaeo-redox and palaeo-salinity conditions. In other words, the fact that the samples in the middle part of the section are rich in OM can depend on the rise in sea level, low-density flows and the provision of a stratified water column. Due to the stratified water column, anoxic conditions may have been temporarily provided, albeit slightly, and OM may have been preserved. Therefore, it is thought that the sea level can be divided into three stages during the deposition of Lutetian clastic rocks. In the I. stage, the sea level is low, there is terrigenous debris matter and low productivity (Fig. 16a). In stage II, the sea level is relatively high, the terrestrial debris material is lower than in stage I and the productivity is higher than in stage I (Fig 16b). Stage III is like stage I, with low sea level, high terrestrial debris material input and low productivity (Fig 16c). However, during the Lutetian, climatic conditions were hot and dry, and chemical weathering was low.

## 6. Conclusion

The following results were reached after a thorough analysis of the geochemical properties of Lutetian shale samples from the Everek area, including elemental composition, C isotopic signature, Rock-Eval parameters, GC and GC-MS saturated and aromatic hydrocarbon parameters.

It was determined that in the HI -$T_{max}$ covariation, 7 shale samples included Type II-III kerogen, while three shale samples included Type II kerogen. $S_2/S_3$ ratios of the analyzed samples are widely distributed and vary between 1.28 and 62.45 and according to various classifications, the kerogen content of these samples varies between Type I and Type III. $\delta_{13}C_{org}$ isotope values ranging between −28.23 and −28.22 support this, which illustrates the low contribution of marine OM and the strong OM intake from land during the deposition of shales. GC parameters such as n-$C_{17}$/n-$C_{27}$, Pr/n-$C_{17}$ - /Ph/n-$C_{18}$ and TAR show that the OM contained in the samples is both terrestrial and marine, but terrestrial OM is more dominant. To clarify the sedimentation environment conditions of the black shales, a variety of biomarker analyses have been conducted. The dominance of $C_{29}$ααα20R steranes over $C_{28}$ααα20R and $C_{27}$ααα20R steranes, low $C_{31}$22R/$C_{30}$H ratios, high $C_{29}/C_{27}$ sterol ratios and the order $C_{29}$MA>$C_{28}$MA>$C_{27}$MA indicate that terrestrial OM is more dominant than marine OM.

Low CIA, C-values, high Th/U ratios (inorganic proxies for palaeo-climate), low Cu/Al, Ni/Al and Zn/Al ratios (inorganic proxies for palaeo-productivity) of the samples indicate hot-arid palaeo-climate conditions and low productivity. The moderate Ti/Al ratios represent moderate terrestrial detrital input during the depositional period. High Ni/Co, Pr/Ph, moderate V/(V+Ni), low Cu/Zn, $C_{35}/C_{34}$ ratios and low HHI values of the shale samples indicate oxic-dyoxic conditions during the Lutetian period. Sr/Ba and TS/TOC ratios showing a wide range indicate that the Lutetian basin changed between freshwater and marine facies and was a terrestrial-marine transition environment. The low gammacerane/C30hopane ratios of the samples also support this.

According to maturity estimations derived from $T_{max}$, calculated vitrinite reflectance values and biomarker maturity criteria, the studied shales have achieved the mature level of the oil window.

Overall, the results obtained, the Lutetian sequence was transported and deposited by low-density turbidite and hyperpycnal turbidite currents. During the deposition of the studied rocks, turbidite flows carried more terrestrial OM to the basin due to hot-dry climate conditions and this caused the amount of terrestrial OM to be more dominant than the marine one. Low-density turbidites contained higher amounts of TOC than hyperpycnal turbidites, suggesting that the turbidite current energy also affects the OM content. In addition, OM enrichment is thought to be controlled by palaeo-redox and palaeo-salinity as well as seawater level.

**Supplementary material.** The supplementary material for this article can be found at https://doi.org/10.1017/S0016756824000281

**Acknowledgements.** The authors gratefully acknowledge Editor Dr. Bas Van de Schootbrugge for editorial handling The authors thank three anonymous reviewers for their constructive comments and suggestions to improve the manuscript.

**Competing interests.** The author declares that I have no known competing financial interests or personal relationships that could have appeared to influence the work reported in this paper.

## References

**Ahmed A, Jahandad S, Hakimi MH, Gharib AF, Mehmood S, Kahal AY and Lashin A** (2022) Organic matter characteristics and conventional oil potentials of shales from the early Jurassic datta formation in the Upper Indus Basin, Northern Pakistan. *Journal of Asian Earth Sciences* **224**, 104975.

**Alexander R, Kagi RI and Sheppard PN** (1983) Relative abundance of dimethylnaphthalene isomers in crude oils. *Journal of Chromatography* **267**, 367–72.

**Algeo TJ and Maynard, JB** (2004). Trace-element behavior and redox facies in core shales of Upper Pennsylvanian Kansas-type cyclothems. *Chemical Geology* **206**, 289–318.

**Bechtel A, Gratzer R and Sachsenhofer RF** (2001) Chemical characteristics of upper cretaceous (Turonian) jet of the gosau group of gams/hieflau (Styria, Austria). *International Journal of Coal Geology* **46**, 27–49.

**Bechtel A, Jia JL, Strobl SAI, Sachsenhofer RF, Liu ZJ, Gratzer R and Püttmann W** (2012) Paleoenvironmental conditions during deposition of the Upper Cretaceous oil shale sequences in the Songliao Basin (NE China): implications from geochemical analyses. *Organic Geochemistry* **46**, 76–95.

**Boon JJ, Hine SH, Burlingame AI, *et al.*** (1983) Organic geochemical studies of Solar Lake laminated cyanobacterial mats. In *Int., Advances in Organic*

*Geochemistry 1981* (Eds. M Bjoray, C. Albrecht, C Cornford, *et al.*, John Wiley & Sons, New York, pp. 207–27.

**Bordenave ML, Espitalié J, Leplat PO, Oudin JL and Vandenbroucke, M.** (1993) Screening techniques for source rock evaluation. In: *Applied Petroleum Geochemistry*, (Eds. M. L. Bordenave) Paris: Editions Technip, pp. 217–78.

**Bourbonniere RA and Meyers PA** (1996) Anthropogenic influences on hydrocarbon contents of sediments deposited in eastern Lake Ontario since 1800. *Environmental Geology* **28**, 22–28.

**Brassell SC and Eglinton G** (1981) Biogeochemical significance of a novel sedimentary C27 stanol. *Nature* **290**, 579–82.

**Brumsack H** (2006) The trace metal content of recent organic carbon-rich sediments: implications for cretaceous black shale formation. *Palaeogeography, Palaeoclimatology, Palaeoecology* **232**, 344–61.

**Buratti N, De Luca R, Garuti L, Sorci A, Spina A and Clayton G** (2024) Thermal maturity evaluation on mildly artificially oxidised sporomorphs: A comprehensive calibration of palynomorph darkness index (PDI) with vitrinite reflectance. *Marine and Petroleum Geology* **162**, 106672.

**Calvert SE and Pedersen TF** (1993) Geochemistry of recent oxic and anoxic marine sediments: implications for the geological record. *Marine Geology* **113**, 67–88.

**Canfield DE** (1994) Factors influencing organic carbon preservation in marine sediments. *Chemical Geology* **114**, 315–29.

**Cao, J., Wu, M., Chen, Y., Hu, K., Bian, L., Wang, L. & Zhang, Y.** 2012. Trace and rare earth element geochemistry of Jurassic mudstones in the northern Qaidam Basin, northwest China. Chemie der Erde Geocemistry 72, 245–252.

**Cardinal D Savoye N, Trull TW, Andre L, Kopczynska EE and Dehairs F** (2005) Variations of carbon remineralisation in the Southern Ocean are illustrated by the Baxs proxy. *Deep-Sea Research I* **52**, 355–70.

**Carroll AR and Bohacs KM** (1999) Stratigraphic classification of ancient lakes: balancing tectonic and climatic controls. *Geology* **27**, 99–102.

**Chandra K, Mishra CS, Samanta U, Gupta A and Mehrotra KL** (1994) Correlation of different maturity parameters in the Ahmedabad–Mehsana Block of the Cambay Basin. *Organic Geochemistry* **21**, 313–21.

**Cirilli S, panfili G, Buratti N and Frixa A** (2018) Paleoenvironmental reconstruction by means of palynofacies and lithofacies analyses: An example from the Upper Triassic subsurface succession of the Hyblean Plateau Petroleum System (SE Sicily, Italy). *Review of Palaeobotany and Palynology* **253**, 70–87.

**Clementz DM, Demaison GJ and Daly AR** (1979) Well Site Geochemistry by Programmed Pyrolysis. Proceedings of the 11th Annual Offshore Technology Conference, Houston, OTC 3410, 1, 465-470.

**Coffin, RB, Fry, B., Peterson, BJ and Wright, RT** (1989) Carbon isotopic compositions of estuarine bacteria. *Limnology and Oceanography* **34**, 1305–10.

**Connan J, Bourouller J, Dessort D and Albrechht P**, (1986) The microbial input in carbonate-anhydrite facies of a sabkha paleoenvironment from Guatemala: a molecular approach. *Organic Geochemistry* **10**, 29–50.

**Cranwell P.A., Eglinton G. and Robinson N**, (1987) Lipids of aquatic organisms as potential contributors to lacustrine sediments-II. *Organic Geochemistry* **11**, 513–27.

**Curiale JA, Cameron D and Davis DV** (1985) Biological marker distribution and significance in oils and rocks of the Monterey Formation, California. *Geochemica et Cosmochimica Acta* **49**, 271–88.

**Dehairs F, Chesselet R and Jedwab J** (1980) Discrete suspended particles of barite and the barium cycle in the open ocean. *Earth and Planetary Science Letters* **49**, 528–50.

**Deng HW and Qian K** (1993) Sedimentary Geochemistry and Environment Analysis. Gansu Technology Publishing House, Lanzhou, pp. 1–150.

**Didyk BM, Simoneit BRT and Brassell SC** (1978) Geochemical Indicators of Paleoenvironmental Conditions of Sedimentation. *Nature* **272**, 216–22.

**Dokuz A, Külekçi E, Aydinçakir E, Kandemir R, Alçiçek MC, Pecha ME and Sünnetçi, K.** (2017) Cordierite-bearing strongly peraluminous Cebre Rhyolite from the eastern Sakarya Zone, NE Turkey: Constraints on the Variscan Orogeny. *Lithos* **278–281**, 285–302.

**Dymond J**, (1981) Geochemistry of Nazca plate surface sediments: an evaluation of hydrothermal, biogenic, detrital, and hydrogenous sources. In *Nazca Plate: Crustal Formation nd Andean Convergence* (Eds. L.V.D. Kulm, J. Dymond, E.J. Dasch, D.M. Hussong and R. Roderick,) p. 133 Geological Society of America. https://doi.org/10.1130/MEM154.

**Dymond J, Suess E and Lyle M** (1992) Barium in deep-sea sediment: a Geochemical proxy for paleoproductivity. *Paleoceanography Paleoclimatology* **7**, 163–81.

**Eglinton G and Hamilton RJ** (1967) Leaf epicuticular waxes. *Science* **156**, 1322–35.

**English J.M., Fowler M, Johnston ST, Mihalynuk MG and Wight KL** (2004) Thermal Maturity in the Central Whitehorse Trough, Northwest British Columbia. Summary of Activities 2004, BC Ministry of Energy and Mines. *Crown Publications, British Columbia*, 79–85.

**Eric BE, Adama A, Etutu EMM, Kwankam FN, Betrant, B. D. and Esue MF** (2023) Paleoclimate characteristics of source area weathering and metallogenic implication of cretaceous black shales in the Mamfe basin, (SW Cameroon): evidence from lithogeochemistry. *Helyon* **9**, e17142.

**Espitalié J, Laporte JL Madec M, Marquis F, Leplat P, Paulet J and Boutefeu A** (1977) Methode rapide de caracterisation des roches meres de leur potentiel petrolier et de leur degre d'evolution. *Revue de l'Institut Francais du Petrole*. **32**, 23–42.

**Eyuboğlu Y, Dudas FO, Thorkelson D, Zhu D-C, Liu Z and Chatterjee N** (2017) Eocene granitoids of northern Turkey: Polybaric magmatism in an evolving arc–slab window system. *Gondwana Research* **50**, 311–45.

**Feng L, Chu X, Zhang Q and Zhang T** (2003) CIA (Chemical index of alteration) and its applications in the Neoproterozoic clastic rocks. *Earth Science Frontiers* **10**, 539–43.

**Ficken KJ, Street-Perrott FA, Perrott RA, Swain DL, Olago DO and Eglinton G** (1998) Glacial/interglacial variations in carbon cycling revealed by molecular and isotope stratigraphy of Lake Nkunga. Mt. Kenya East Africa. *Organic Geochemistry* **29**, 1701–19.

**Fu X, Wang J, Chen W, Feng X, Wang D, Song C and Zeng S** (2016) Elemental geochemistry of the early Jurassic black shales in the Qiangtang Basin, eastern Tethys: constraints for palaeoenvironment conditions. *Geological Journal* **51**, 443–54.

**Gani MR** (2004) From turbid to lucid: a straight forward approach to sediment gravity flows and their deposits. *Sedimentary Record* **2**, 4–8.

**George SC, Ruble TE, Dutkiewicz A and Eadington PJ** (2001) Assessing the maturity of oil trapped in fluid inclusions using molecular geochemistry data and visually-determined fluorescence colors. *Applied Geochemistry* **16**, 451–73.

**Goldberg ED and Arrhenius GOS** (1958) Chemistry of Pacific pelagic sediments. *Geochimica et Cosmochimica Acta* **13**, 158–212.

**Goldberg K and Humayun M**, (2010) The applicability of the Chemical Index of Alteration as a paleoclimatic indicator: an example from the Permian of the Parana Basin, Brazil. *Palaeogeography, Palaeoclimatology, Palaeoecology* **293**, 175–83.

**Gücer MA** (2021) Origin, petrogenesis and geodynamic implications of the early Eocene Altınpınar adakitic andesites in the eastern Sakarya Zone, northeastern Turkey. Chem- Erde-*Geochemistry* **81**, 125766.

**Güven IH** (1993) *1/100000 scaled geological map series of Turkey* No:57-60 MTA Publication, Ankara

**Hakimi MH, Abdullah, WH and Shalaby MR** (2011) Organic geochemical characteristics of crude oils from the Masila Basin, eastern Yemen. *Organic Geochemistry* **42**, 465–76.

**Hartkopf-Fröder C, Königshof P, Littke R and schwarzbauer J** (2015) Optical thermal maturity parameters and organic geochemical alteration at low grade diagenesis to anchimetamorphism: a review. *International Journal Coal Geology* **150-151**, 74–119.

**Hatch JR and Leventhal JS**, (1992) Relationship between inferred redox potential of the depositional environment and geochemistry of the upper Pennsylvanian (Missourian) Stark shale member of the Dennis limestone, Wabaunsee County, Kansas, USA. *Chemical Geology* **99**, 65–82.

**Hatem BA Abdullah WH, Hakimi MH, Mustapha KA** (2016) Origin of organic matter and paleoenvironment conditions of the Late Jurassic organic-rich shales from Shabwah sub-basin (western Yemen): Constraints from petrology and biological markers. *Marine and Petroleum Geology* **72**, 83–97.S

**He J, Ding W, Jiang Z, Jiu K, Li A and Sun Y** (2017) Mineralogical and chemical distribution of the Es3L oil shale in the Jiyang Depression,

Bohai Bay Basin (E China): Implications for paleoenvironmental reconstruction and organic matter accumulation. *Marine and Petroleum Geology* **81**, 196–219.

**Hu J, Li Q, Song C, Wang S and Shen B** (2017) Geochemical characteristics of the Permian sedimentary rocks from Qiangtang Basin: constraints for paleoenvironment and paleoclimate. *Terrestrial, Atmospheric and Oceanic Sciences* **28**, 271–82.

**Huang H, Larter SR and Love GD** (2003) Analysis of wax hydrocarbons in petroleum source rocks from the Damintun depression, eastern China, using high-temperature gas chromatography. *Organic Geochemistry* **34**, 1673–168.

**Huang WY and Meinschein WG** (1979) Sterols as ecological indicators. *Geochimica et Cosmochimica Acta* **43**, 739–45.

**Huang Y, Dupont L, Sarnthein M, Hayes JM and Eglinton G** (2000) Mapping of C4 plant input from North West Africa into North East Atlantic sediments. *Geochimica Et Cosmochimica Acta* **64**, 3505–13.

**Hunt JM** (1996) *Petroleum Geochemistry and Geology*. W.H. Freeman and Company, New York.

**Ilevbare M and Adeleye RA** (2023) Paleoenvironment of deposition and hydrocarbon potential of Maastritchian Shale Sediments, Southern Anambra Basin, Edo State, Nigeria. *Arabian Journal of Geosciences* **16**, 607.

**Jarvie DM, Claxton BL, Henk F and Breyer JT** (2001) Oil and shale gas from the Barnett Shale, Ft, Worth Basin, Texas (abs), *AAPG Annual Meeting Program*, pp. A100.

**Jarvie DM, Hill RJ, Ruble TE and Pollastro RM** (2007) Unconventional shale-gas systems: The Mississippian Barnett Shale of north-central Texas as one model for thermogenic shale-gas assessment. *AAPG Bulletin* **91**, 475–99.

**Jones B and Manning DA** (1994) Comparison of geochemical indices used for the interpretation of palaeoredox conditions in ancient mudstones. *Chemical Geology* **111**, 111–29.

**Kaygusuz A and Öztürk M**, (2015) Geochronology, geochemistry, and petrogenesis of the Eocene Bayburt intrusions, Eastern Pontide, NE Turkey: implications for lithospheric mantle and lower crustal sources in the high-K calc-alkaline magmatism. *Journal of Asian Earth Sciences* **108**, 97–116.

**Kaygusuz A, Yücel C, Aydinçakir E, Gücer MA and Ruffet G** (2022) $^{40}$Ar–$^{39}$Ar dating, whole–rock and Sr–Nd isotope geochemistry of the Middle Eocene calc–alkaline volcanic rocks in the Bayburt area, Eastern Pontides (NE Turkey): Implications for magma evolution in an extension–related setting. *Mineralogy and Petrology* **116**, 379–99.

**Keskin İ, Korkmaz S, Gedik İ, Ateş M, Gök L, Küçümen Ö and Erkal T** (1990) *Geology of Bayburt region*, MTA report Ankara, No: 8995.

**Kidder D, Xa L, Erwin D and Xa H**, (2001) Secular distribution of biogenic silica through the phanerozoic: comparison of silica 2010; replaced fossils and bedded cherts at the series level. *Journal of Geology* **109**, 509–22.

**Killops S and Killops V** (2005) *Introduction to Organic Geochemistry*, second ed. Blackwell Publishing, Oxford.

**Koralay DB** (2021) Investigation of the paleodepositional environment of the Middle Miocene aged organic matter-rich rocks (Tavas/Denizli/SW Turkey) by using biomarker parameters and stable isotope compositions ($^{13}$C and $^{15}$N). *Bulletin Mineral Research Exploration* **164**, 39–52.

**Köster J, Van Kaam-Peters HM, Koopmans MP, De Leeuw JW and Damsté JSS** (1997) Sulphurisation of homohopanoids: Effects on carbon number distribution, speciation, and 22S22R epimer ratios. *Geochimica et Cosmochimica Acta* **61**, 2431–52.

**Kostova I, Zdravkov A, Bechtel A, Botoucharov N, Grob D, Dochev D and Apostolova D** (2022) Characterization of organic matter from the Cretaceous sedimentary and volcano-sedimentary strata from Livingston Island, Antarctic Peninsula: Insights from organic petrology, molecular proxies and carbon and hydrogen isotopes. *International Journal of Coal Geology*, **252**, 103940.

**Kumar D, Ghosh S, Tiwari B, Varma AK, Mathews RP and Chetia R.** (2021) Palaeocene-Eocene organic sedimentary archives of Bikaner-Nagaur Basin, Rajasthan, India: An integrated revelation from biogeochemical and elemental proxies. *International Journal of Coal Geology*, **247**, 103848.

**Lafargue E, Marquis F and Pillot D** (1998) Rock-Eval 6 applications in Hydrocarbon Exploration, production, and Soil Contamination Studies. *Oil Gas Science Technology* **53**, 421–37.

**Lamb AL, Wilson GP and Leng MJ** (2006) A review of coastal palaeoclimate and relative sea-level reconstructions using δ13C and C/N ratios in organic material. *Earth-Science Reviews* **75**, 29–57.

**Li M, Zhang S, Snowdon L and Issler D.** (2008) Oil-source correlation in Tertiary deltaic petroleum systems: a comparative study of the Beaufort-Mackenzie Basin in Canada and the Pearl River Mouth Basin in China. *Organic Geochemistry*. **39**, 1170–75.

**Li Q, Wu SH, Xia DL, You XL, Zhang HM and Lu H**, (2020) Major and trace element geochemistry of the lacustrine organic-rich shales from the Upper Triassic Chang 7 Member in the southwestern Ordos Basin, China: implications for paleoenvironment and organic matter accumulation. *Marine and Petroleum Geology* **111**, 852–67.

**Li TY, HE S and Yang Z** (2008) The marine source rock formation conditions and control factors. *Geological Science and Technology Information* **27**, 63–70. (in Chinese with English abstract).

**Liang C, Wu J, Jiang Z, Cao Y and Song G** (2018) Sedimentary environmental controls on petrology and organic matter accumulation in the upper fourth member of the Shahejie Formation (Paleogene, Dongying depression, Bohai Bay Basin, China). *International Journal of Coal Geology*. **186**, 1–3.

**Liang H, Xu G, Xu F, Yu Q, Liang J and Wang D** (2020) Paleoenvironmental evolution and organic matter accumulation in an oxygen-enriched lacustrine basin: A case study from the Laizhou Bay Sag, southern Bohai Sea (China). *International Journal of Coal Geology*, **217**, 103318.

**Lin XH, Zhan ZW, Zou YR, Cai YL, Liang T and Shi J.** (2019) Elemental geochemical characteristics of the Lucaogou Formation oil shale in the southeastern Junggar Basin and its depositional environmental implications. *Geochimica* **048**, 67–78.

**Makeen Y M, Hakimi MH and Abdullah WH** (2015). The origin, type and preservation of organic matter of the Barremian-Aptian organic-rich shales in the Muglad Basin, Southern Sudan, and their relation to paleoenvironmental and paleoclimate conditions. *Marine and Petroleum Geology* **65**, 187–97.

**Mallick M, Banerjee B, Hassan T, Kumar TV, Babu EVSSK, Krishna K and Kumar R** (2022) Geochemistry of Permian carbonaceous shales from Raniganj sub-basin, Damodar Valley, India: implications for provenance, weathering, tectonics and source of organic matter. *Applied Geochemistry* **146**, 105469.

**Martin JH and Knauer GA** (1973) The elemental composition of plankton. *Geochimica et Cosmochimica Acta* **37**, 1639–53.

**Mckay JL, Pedersen TF and Mucci A** (2007) Sedimentary redox conditions in continental margin sediments (N.E. Pacific) - influence on the accumulation of redox-sensitive trace metals. *Chemical Geology* **238**, 180–96.

**Mclennan SM, Hemming S, Mcdaniel DK and Hanson GN.** (1993) Geochemical approaches to sedimentation, provenance, and tectonics. In *Processes controlling the composition of clastic sediments* (eds MJ Johnson and A Basu), pp.21–40. Geological Society of America, Special Papers, 285

**Mello MR and Maxwell JR** (1990) Organic geochemical and biological marker characterization of source rocks and oils from lacustrine environments in the Brazilian Continental Margin. *In: Lacustrine Basin Exploration*. (Eds. BJ Katz), pp. 77–97. Tulsa, OK, USA: AAPG Memoirs.

**Meng Q, Liu Z, Bruch AA, Liu R and Hu F** (2012) Palaeoclimatic evolution during Eocene and its influence on oil shale mineralization, Fushun basin, China. *Journal of Asian Earth Sciences* **45**, 95–105.

**Meyers PA** (2003) Applications of organic geochemistry to paleolimnological reconstructions: a summary of examples from the Laurentian Great Lakes. *Organic Geochemistry* **34**, 261–89.

**Meyers PA and ishiwatari R** (1993) Lacustrine organic geochemistry—an overview of indicators of organic matter sources and diagenesis in lake sediments. *Organic Geochemistry* **20**, 867–900.

**Moldowan JM, Sundararaman P. and Schoell M** (1986) Sensitivity of biomarker properties to depositional environment and/or source input in the lower Toarcian of SW-Germany. *Organic Geochemistry* **10**, 915–26.

**Mukhopadhyay PK, Wade JA and Kruge MA** (1995) Organic facies and maturation of Jurassic/Cretaceous rocks, and possible oil-source rock correlation based on pyrolysis of asphaltenes, Scotion Basin, Canada. *Organic Geochemistry* **22**, 85–104.

https://doi.org/10.1017/S0016756824000281 Published online by Cambridge University Press

**Murphy A.E., Sageman BB, Hollander DJ and Lyons TW** (2000) Black shale deposition and faunal overturn in the Devonian Appalachian Basin: clastic starvation, seasonal water-column mixing, and efficient biolimiting nutrient recycling. *Paleoceanography* **15**, 280–91.

**Musaoğlu A** (1987) *Bayburt-Maden Kop Region Geology and Mining Projection Report*, MTA General Directorate Compilation Report no: 8541, Ankara.

**Mutti E, Bernoulli D and Lucchi FR** (2009) Turbidites and turbidity currents from Alpine flysch to the exploration of continental margins. *Sedimentology* **56**, 267–318.

**Nesbitt HW and Young GM** (1982) Early Proteozoic climate and plate motions inferred from major element chemistry of lutites. *Nature* **299**, 715–17.

**Ortiz JE., Torres T, Delgado A, Llamas FJ and Valle M** (2010) Palaeoenvironmental changes in the Padul Basin (Granada, Spain) over the last 1 Ma B.P. based on the biomarker content. *Palaeogeography, Palaeoclimatology, Palaeoecology* **298**, 286–99.

**Ortiz JE, Torres T, Delgado D, Valle M, Soler V, Araujo R, Rivas MR, Julià R, Sanchez-Palencia Y and Vega-Panizo R** (2021) Bulk and compound-specific δ13C and *n*-alkane indices in a palustrine intermontane record for assessing environmental changes over the past 320 ka: the Padul Basin (Southwestern Mediterranean realm). *Journal of Iberian Geology* **47**, 625–39.

**Peters KE and Cassa MR** (1994) Applied source rock geochemistry. *In the petroleum system from source to trap* (Eds. L.B. Magoon and W.G. Dow) AAPG Memoir, 60, p. 93–120.

**Peters KE and Moldowan JM** (1993) *The Biomarker Guide, Interpreting Molecular Fossils in Petroleum and Ancient Sediments*. Englewood Cliff, New Jersey: Prentice Hall. pp. 63.

**Peters KE, Walters CC and Moldowan JM** (2005) *The Biomarker Guide*. Volume 2. In: *Biomarkers and Isotopes in Petroleum Exploration and Earth History*. pp. 633–634. Cambridge, UK: Cambridge University Press.

**Philp PR** (1994) Geochemical characteristics of oils derived predominantly from terrigenous source materials. In. *Coal and Coal-Bearing Strata as Oil-Prone Source Rocks?* (eds AC Scot, AJ Fleet,) Special Publications No. 77. pp. 71–91. London, UK: Geological Society.

**Piper DZ and Perkins RB** (2004) A modern vs. Permian black shale— the hydrography, primary productivity, and water-column chemistry of deposition. *Chemical Geology* **206**, 177–97.

**Powell TG and Mckirdy DM** (1973) Relationship between ratio of pristane to phytane, crude oil composition and geological environment in Australia. *Nature Physical Science* **243**, 37–39.

**Qiao, J., Baniasad, A., Zieger,L., Zhang, L., Luo, Q. and Littke, R.** (2021) Paleo-depositional environment, origin and characteristics of organic matter of the Triassic Chang 7 Member of the Yanchang Formation throughout the mid-western part of the Ordos Basin, China. *International Journal of Coal Geology* **237**, 103636.

**Radke M** (1987) Organic geochemistry of aromatic hydrocarbons. *Advances in petroleum geochemistry* **2**, 141–207.

**Radke M and Willsch H** (1994) Extractable Alkldibenzothiophenes in Posidonia Shale (Toarcian) Source Rocks: Relationship of Yields to Petroleum Formation and Expulsion. *Geochimica et Cosmochimica Acta* **23**, 5223–44.

**Riboulleau A, Spina A, Vecoli M, Riquier L, Quijada M, Tribovillard N and Averbuch O** (2018) Organic matter deposition in the Ghadames Basin (Libya) during the Late Devonian—A multidisciplinary approach. *Palaeogeography, palaeoclimatology, palaeoecology* **497**, 37–51.

**Rimmer SM** (2004) Geochemical paleoredox indicators in Devonian–Mississippian black shales, Central Appalachian Basin (USA). *Chemical Geology* **206**, 373–91.

**Rohmer M and OURISSON G** (1976) D´eriv´es du bact´eriohopane: variations structurales et r´epartition. *Tetrahedron Letters* **17**, 3637–40.

**Samanta A, Bera, M.K., Ghosh, R., Bera, S., Filley, T., Pande, K., Rathore, S.S., Rai, J. and Sarkar, A.** (2013) Do the large carbon isotopic excursions in terrestrial organic matter across Paleocene–Eocene boundary in India indicate intensification of tropical precipitation? *Palaeogeography, Palaeoclimatology, Palaeoecology* **387**, 91–103.

**Saydam Eker C** (2012) Petrography and geochemistry of Eocene sandstones from eastern Pontides (NE Turkey): Implications for source area weathering, provenance and tectonic setting. *Geochemistry International* **50**, 683–701.

**Saydam Eker C** (2013) Organic Geochemical Characteristics and Depositional Environments of the Eocene Deposits in the Eastern Black Sea Region, NE Turkey. *Energy Sources, Part A: Recovery, Utilization, and Environmental Effects* **35**, 413–25.

**Saydam Eker Ç** (2022) Geochemical properties of Eocene Turbiditic Sequence from Bayburt (NE Turkey): Organic matter input, paleoenvironment and paleoclimatic conditions. *Arabian Journal of Geosciences*, **15**, 1733.

**Saydam Eker Ç., Akpinar, I. and Sipahi, F.** (2016a) Organic geochemistry and element distribution in coals formed in Eocene Lagoon facies from the Eastern Black Sea Region, NE Turkey, *Turkish Journal of Earth Science* **25**, 467–89.

**Saydam Eker Ç., Akpinar İ., Sipahi F. and Yapici E.** (2016b) Concentrations of Elements in Lias Coals from the Eastern Black Sea Region, NE-Turkey. *Energy Sources, Part A: Recovery, Utilization, and Environmental Effects* **38**, 1643–52.

**Saydam Eker Ç and Ari UV** (2020) Geochemistry of the Middle Jurassic sediments in Gümüşhane, north-eastern Turkey: Implications for weathering and provenance: *Geological Journal* **55**, 4954–76.

**Saydam Eker Ç. and Demirkol, Kiliç, E.** (2018) Geochemistry of Çoruh River bed sediments in NE Turkey: Implications in weathering-sedimentary cycle, provenance, and metal pollution. *Geochemistry International* **56**, 579–600.

**Saydam Eker, Ç. and Demirkol, Kiliç, E.** (2024) Pollution level, environmental risk, and source of potentially toxic elements in the sediment of Çoruh River (Bayburt, NE Türkiye). *Arabian Journal of Geosciences* **17**, 52.

**Saydam Eker Ç., Sipahi F. and AKPINAR I.** (2015) Organic Maturity and Hydrocarbon Potential of Liassic Coals from the Eastern Pontides, NE Turkey. *Energy Sources, Part A: Recovery, Utilization, and Environmental Effects* **37**, 1260–67.

**Scalan RS and Smith JE** (1970) An improved measure of the odd-even predominance in the normal alkanes of sediment extracts and petroleum. *Geochimica et cosmochimica acta* **34**, 611–20.

**Schito A, Corrado S, Trolese M, Aldega L, Caricchi C, Cirilli S and Valentim B** (2017) Assessment of thermal evolution of Paleozoic successions of the Holy Cross Mountains (Poland). *Marine and Petroleum Geology* **80**, 112–32

**Schoepfer SD, Shen, J., Wei, H.Y., Tyson, R.V., Ingall, E., Algeo, T. J.** (2015) Total organic carbon, organic phosphorus, and biogenic barium fluxes as proxies for paleo-marine productivity. *Earth-Science Reviews* **149**, 23–52.

**Seifert WK and Moldowan JM**, (1978) Applications of steranes, terpanes and monoaromatics to the maturation, migration and source of crude oils. *Geochimica et Cosmochimica Acta* **42**, 77–95.

**Seifert WK and Moldowan JM** (1986) Use of biological markers in petroleum exploration. *Methods in geochemistry and geophysics* **24**, 261–90.

**Shanmugam G** (1985) Significance of Coniferous rain Forests and Related Organic Matter in Generating Commercial Quantities of Oil, Gippsland Basin, Australia1. *AAPG Bulletin* **69** (8), 1241–54

**Shen J, Schoepfer SD, Feng Q, Zhou L, Yu J, Song H, Wei H and Algeo TJ** (2015) Marine productivity changes during the end-Permian crisis and Early Triassic recovery. *Earth-Science Reviews* **149**, 136–62.

**Sim MS, Bosak T and Ono S** (2011) Large sulfur isotope fractionation does not require disproportionation. *Science* **333**, 74–77.

**Sinninghe Damste JS, Verschuren D, Ossebaar J, Blokker J, Van Houten R, Van Der Meer MTJ, Plessen B and Schouten S** (2011) A 25,000-year record of climate-induced changes in lowland vegetation of eastern equatorial Africa revealed by the stable carbon-isotopic composition of fossil plant leaf waxes. *Earth and Planetary Science Letters* **302**, 236–46.

**Sorci A, Cirilli S, Clayton G, Corrado S, Hints O, Goodhue R, Schito A and Spina A** (2020) Palynomorph optical analyses for thermal maturity assessment of Upper Ordovician (Katian-Hirnantian) rocks from Southern Estonia. *Marine Petroleum Geology* 120(4), 104574.

**Spina A, Cirilli S, Sorci A, Schito A, Clayton G, Corrado S, Fernandes P, Galasso F, Montesi G, Pereira Z, Rashidi M and Rettori R**, (2021) Assessing thermal maturity through a multi-proxy approach: a case study from the Permian Faraghan formation (Zagros Basin, Southwest Iran). *Geoscience* 11(12), 484.

**Spina A, Vecoli M, Riboulleau A, Clayton G, Cirilli S, Di Michele A, Marcogiuseppe A, Rettori R, Sassi P, Servais T and Riquier L** (2018)

https://doi.org/10.1017/S0016756824000281 Published online by Cambridge University Press

Application of Palynomorph Darkness Index (PDI) to assess the thermal maturity of palynomorphs: A case study from North Africa. *International Journal of Coal Geology* **188**, 64–78.

**Street-Perrott FA, Huang Y, Perrott RA, Eglinton, G, Barker P, Ben Khelifa, L., Harkness, D. D. and Olago, D.** (1997) Impact of lower atmospheric CO2 on tropical mountain ecosystems: carbon-isotope evidence. *Science* **278**, 1422–26.

**Sun Q, Xie M, Shi L, Zhang Z, Lin Y, Shang W, Wang K, Li W, Liu J and Chu G** (2013) Alkanes, compound-specific carbon isotope measures and climate variation during the last millennium from varved sediments of Lake Xiaolongwan, northeast China. *Journal of Paleolimnology* **50**, 331–44.

**Tanaka K, Akagawa F, Yamamoto K, Tani, Y., Kawabe, I. and Kawai, T** (2007) Rare earth element geochemistry of Lake Baikal sediment: its implication for geochemical response to climate change during the Last Glacial/Interglacial transition. *Quaternary Science Reviews* **26**, 1362–68.

**Tao S, Wang C, Du J., Liu L and Chen, Z** (2015) Geochemical application of tricyclic and tetracyclic terpanes biomarkers in crude oils of NW China. *Marine and Petroleum Geology* **67**, 460–467.

**Tissot BP and Welte DH** (1984) *Petroleum Formation and Occurence*. Springer Verlag, Berlin Heidelberg, New York, Tokyo.

**Topuz G, Altherr R, Kalt, A., Satir, M., Werner, O**. and Schwarz, W. (2004) Aluminous granulites from the Pulur complex, NE Turkey: a case of partial melting, efficient melt extraction and crystallization. *Lithos* **72**, 183–207.

**Tribovillard N, Algeo TJ, Lyons T and Riboulleau A** (2006) Trace metals as paleoredox and paleoproductivity proxies: an update. *Chemical Geology* **232**, 12–32.

**Tripathy GR, Singh SK and Ramaswamy V** (2014) Major and trace element geochemistry of Bay of Bengal sediments: implications to provenances and their controlling factors. *Palaeogeography, Palaeoclimatology, Palaeoecology* **397**, 20–30.

**Trudinger PA, Chambers LA and Smith JW** (1985) Low-temperature sulphate reduction: biological versus abiological. *Canadian Journal of Earth Sciences* **22**, 1910–18.

**Volkman JK** (2003). Sterols in microorganisms. *Applied Microbiology and Biotechnology* **60**, 495–506.

**Volkman JK, Barrett SM and Blackburn SI** (1999) Eustigmatophyte microalgae are potential sources of C29 sterols, C22–C28 n-alcohols and C28–C32 n-alkyl diols in freshwater environments. *Organic Geochemistry* **30**, 307–18.

**Wang, Z., Fu, X., Feng, X., Song, C., Wang, D., Chen, W. and Zeng, S.** (2017) Geochemical features of the black shales from the Wuyu Basin, southern Tibet: implications for palaeoenvironment and palaeoclimate. *Geological Journal* **52,** 282–97.

**Waples DW and Machihara TM** (1991) Biomarkers for Geologists. AAPG Methods in Exploration Series No. 9. American Association of Petroleum Geologists, Tulsa, Oklahoma.

**Wei, W. and Algeo, T.J.** (2020) Elemental proxies for paleosalinity analysis of ancient shales and mudrocks. *Geochimica et Cosmochimica Acta* **287**, 341–66.

**Welte DH and Ebhardt G** (1968) Distribution of long chain *n*-paraffins and *n*-fatty acids in sediments from the Persian Gulf. *Geochimica et Cosmochimica Acta* **32**, 465–66.

**Welte DH and Waples DW** (1973) Über die Bevorzugung geradzahliger n-Alkane in Sedimentgesteinen. *Die Naturwissenschaften* **60**, 516–17.

**Whiticar MJ** (1996) Stable isotope geochemistry of coals, humic kerogens and related natural gases. *International Journal of Coal Geology* **32**, 191–215.

**Wignall PB** (1994) *Black Shales*, Clarendon Press, Oxford, 127.

**Wu, Z., Zhao, X., Wang, E., Pu, X., Lash, G., Han, W., Zhang, W. and Feng, Y.** (2021) Sedimentary environment and organic enrichment mechanisms of lacustrine shale: A case study of the Paleogene Shahejie Formation, Qikou Sag, Bohai Bay Basin. *Paleogeography, Palaeoclimatology, Palaeoecology* **573**, 110404.

**Xie, S., Guo, J., Huang, J., Chen, F., Wang, H. and Farrimond, P.** (2004) Restricted utility of δ13C of bulk organic matter as a record of paleovegetation in some loess–paleosol sequences in the Chinese Loess Plateau. *Quaternary Research* **62**, 86–93.

**Xu, G., Hannah, J.L., Bingen, B., Georgiev, S. and Stein, H.J.** (2012) Digestion methods for trace element measurements in shales: paleoredox proxies examined. *Chemical Geology* **324–325**, 132–147.

**Xu, J., Liu, Z., Bechtel, A., Meng, Q., Sun, P., Jia, J., Cheng, L. and Song, Y.** (2015) Basin evolution and oil shale deposition during Upper Cretaceous in the Songliao Basin (NE China): Implications from sequence stratigraphy and geochemistry. *International Journal of Coal Geology*. **149**, 9–23.

**Xu, X**. and Shao, L. (2018) Limiting factors in utilization of chemical index of alteration of mudstones to quantify the degree of weathering in provenance. *Journal of Palaeogeography* **20**, 515–22.

**Yadav S and Rajamani V** (2004) Geochemistry of aerosols of northwestern part of India adjoining the Thar Desert. *Geochimica et Cosmochimica Acta* **68**, 1975–88.

**Yan D., Chen D., Wang Q and Wang J** (2010) Large-scale climatic fluctuations in the latest Ordovician on the Yangtze block, South China. *Geology* **38**, 599–602.

**Yang T, Cao Y and Wang Y** (2015) Status and trends in research on deep - water gravity flow deposits. *Acta Geologica Sinica* (English edition) **89**, 610–31.

**Zhang P Meng Q., Misch D, Sachsenhofer R, Liu Z, Hu F and Shen L** (2021) Oil shale potential of the lower cretaceous Jiufotang Formation, Beipiao Basin, Northeast China. *International Journal of Coal Geology* **236**,103640.

**Zhang S, Wang X, Wang H, Bjerrum C, Hammarlund E, Haxen E, Wen H, Ye Y and Canfield D** (2019). Paleoenvironmental proxies and what the Xiamaling Formation tells us about the mid-Proterozoic ocean. *Geobiology* **17** 1–22.

**Zhang SH, Liu, CY, Liang H, Wang JQ, Bai JK, Yang MH, Liu GH, Huang H X and Guan YZ** (2018) Paleoenvironmental conditions, organic matter accumulation, and unconventional hydrocarbon potential for the Permian Lucaogou Formation organic-rich rocks in Santanghu Basin, NW China. *International Journal of Coal Geology* **185**, 44–60.

**Zhao Z, Zhao J, Wang H, Liao J and Liu C**, (2007) Distribution characteristics and applications of trace elements in Junggar Basin (in Chinese with English abstract). *Natural Gas Exploration and Development* **30**, 30–33.

**zhou W, Xie S, Meyers PA and Zheng Y** (2005) Reconstruction of late glacial and Holocene climate evolution in southern China from geolipids and pollen in the Dingnan peat sequence. *Organic Geochemistry* **36**, 1272–84.

**Zhou K, Sun J, Yang M, Zhang S, Wang W, Gao R, Zhang P, Wang W, Liu H, Shao L. and Lu J** (2023) Geochemical Characteristics of the Middle Jurassic Coal-Bearing Mudstones in the Dameigou Area (Qaidam Basin, NW China): Implications for Paleoclimate, Paleoenvironment, and Organic Matter Accumulation. *American Chemical Society*, https://doi.org/10.1021/acsomega.3c05433.

**Zonneveld KAF, Versteegh GJM, Kasten S, Eglinton TI, Emeis KC, Huguet C, Koch, B.P., De Lange, G.J., De Leeuw, J.W. Middelburg, J.J., Mollenhauer, G., Prahl, F.G., Rethemeyer, J. and Wakeham, S.G.** (2010) Selective preservation of organic matter in marine environments; processes and impact on the sedimentary record. *Biogeosciences* **7**, 483–511.

https://doi.org/10.1017/S0016756824000281 Published online by Cambridge University Press